LEONARDO FISCHI SOMMER

EMG-DRIVEN EXOSKELETON CONTROL

São Paulo
2019

LEONARDO FISCHI SOMMER

EMG-DRIVEN EXOSKELETON CONTROL

Dissertation presented to Escola Politécnica of University of São Paulo, to obtain the title of Master in Science

São Paulo
2019

LEONARDO FISCHI SOMMER

EMG-DRIVEN EXOSKELETON CONTROL

Dissertation presented to Escola Politécnica of University of São Paulo, to obtain the title of Master in Science

Field of Knowledge:
Control and Mechanical Automation Engineering

Supervisor:
Prof. Dr. Arturo Forner Cordero

São Paulo
2019

Autorizo a reprodução e divulgação total ou parcial deste trabalho, por qualquer meio convencional ou eletrônico, para fins de estudo e pesquisa, desde que citada a fonte.

Este exemplar foi revisado e corrigido em relação à versão original, sob responsabilidade única do autor e com a anuência de seu orientador.

São Paulo, 25 de Julho de 2019

Assinatura do autor:

Assinatura do orientador:

Catalogação-na-publicação

Sommer, Leonardo
EMG-DRIVEN EXOSKELETON CONTROL / L. Sommer -- versão corr. -- São Paulo, 2019.
109 p.

Dissertação (Mestrado) - Escola Politécnica da Universidade de São Paulo. Departamento de Engenharia Mecânica.

1.CONTROLE (TEORIA DE SISTEMAS E CONTROLE) 2.ELETROMIOGRAFIA 3.BIOMECÂNICA 4.IDENTIFICAÇÃO DE SISTEMAS I.Universidade de São Paulo. Escola Politécnica. Departamento de Engenharia Mecânica II.t.

ACKNOWLEDGMENTS

To Iris and my family, for their endless support.

To Professor Arturo Forner Cordero, for the guidance.

To Professor Rafael, Cauê, Carlos, Franklin, Lucas, Rafael and my other colleagues from the Biomechatronics Laboratory, for their companionship and contribution to this work.

"It is not the critic who counts; not the man who points out how the strong man stumbles, or where the doer of deeds could have done them better. The credit belongs to the man who is actually in the arena, whose face is marred by dust and sweat and blood; who strives valiantly; who errs, who comes short again and again, because there is no effort without error and shortcoming; but who does actually strive to do the deeds; who knows great enthusiasms, the great devotions; who spends himself in a worthy cause; who at the best knows in the end the triumph of high achievement, and who at the worst, if he fails, at least fails while daring greatly, so that his place shall never be with those cold and timid souls who neither know victory nor defeat."

-- Theodore Roosevelt

RESUMO

A necessidade por mecanismos que auxiliam os movimentos do ser humano vem crescendo devido ao aumento do número de pessoas portadores de deficiências que afetam a capacidade motora. Nesse cenário, é de grande importância o desenvolvimento de métodos de controle que auxiliem a interface entre o dispositivo de assistência motora e o seu usuário. Esse trabalho propõe um controlador para um exoesqueleto com um grau de liberdade, usando sinais de eletromiografia de superfície do usuário como sinal de entrada. Um exoesqueleto foi adaptado para servir de plataforma para o método de controle desenvolvido. Para criar um modelo EMG-ângulo, um conjunto de experimentos foi conduzido com seis voluntários. O experimento consistiu em uma série de movimentos de flexo-extensão do cotovelo contínuos e discretos com diferentes níveis de carga. Utilizando os dados do experimento, métodos de identificação de sistemas linear (ARIMAX) e não linear (Hammerstein-Wiener) foram avaliados para determinar qual o melhor candidato para a estimação do modelo EMG-Ângulo, baseado em sua acurácia e facilidade de implementação. Um novo experimento foi conduzido para desenvolver um controlador em tempo real, baseado no modelo FIR e testado em uma aplicação em tempo real. Testes indicaram que o controlador é capaz de estimar o ângulo da junta do cotovelo com valores de correlação acima de 70% e raiz do erro quadrático médio menor que 25°, quando comparados aos valores medidos de ângulo da junta do cotovelo.

Palavras-Chave – Exoesqueleto, EMG, Eletromiografia, Controle proporcional, Identificação de sistemas.

ABSTRACT

The need for mechanisms that assist human movements has been increasing due to the rising number of people that has some kind of movement disability. In this scenario, it is of great importance the development of control methods that assist the interface between a motor assistive device and its user. This work proposes a controller for an exoskeleton with one degree of freedom, using surface electromyography signals from the user as the input signal. An exoskeleton was adapted to serve as platform for the developed control method. To create an EMG-to-Angle model, a set of experiments were carried out with six subjects. The experiment consisted of a series of continuous and discrete elbow flexion and extension movements with different load levels. Using the experimental data, linear (ARIMAX) and non linear (Hammerstein-Wiener) system identification methods were evaluated to determine which is the best candidate for the estimation of the EMG-to-Angle model, based on its accuracy and ease of implementation. A new experiment was conducted to develop a real-time controller, based on FIR model and tested in a real-time application. Tests showed that the controller is capable of estimating the elbow joint angle with correlation above 70% and root-mean-square error below 25° when compared to the measured elbow joint angles.

Keywords – Exoskeleton, EMG, Electromyography, Proportional control, System identification.

LIST OF FIGURES

1 Illustration of the myopulse processing technique. The upper trace shows a typical bandpass-filtered EMG signal recorded with surface electrodes. The output will remain off as long as the absolute value of the EMG signal in the upper trace is below the level δ, otherwise the output will be turned on. The lower trace illustrates the output from the myopulse processor (Source: PHILIPSON, 1985) 18

2 Diagram showing the possible movement areas according to the muscle inputs (Source: PHILIPSON, 1985) 19

3 Average of the first 300ms of the EMG recordings for the following movements: For a healthy subject: a) Isometric contraction; b) elbow flexion; c) Forearm supination; d) elbow extension; e) wrist flexion; f) forearm pronation; for the amputee subject: g) inward humeral rotation; h) contraction of the flexor muscle group; i) contraction of the extensor muscle group and j) biceps/triceps co-contraction (Adapted from HUDGINS; PARKER; SCOTT, 1993). 21

4 HAL-5 exoskeleton (Source: SANKAI, 2011) 26

5 University of California at Berkeley's BLEEX exoskeleton (Source: ZOSS; KAZEROONI; CHU, 2006) 27

6 The ReWalk^{TM} exoskeleton worn by an user and its basic structure (Source: ESQUENAZI, 2013) 29

7 Visual representation of framework/methodology 33

8 Assemble of the ETMICAE 36

9 Base 37

10 Hip abduction/adduction joint 37

11 Hip plate 38

12 Hip flexion/extension joint 38

13 Thigh and leg bars 39

14 Knee flexion/extension joint 39

15 Upper limb exoskeleton with one degree of freedom (Source: SOMMER, 2015) 40

16 Power Window Lifter (Source: SOMMER, 2015) 41

17 Schematic of the electronics (Source: SOMMER, 2015) 42

18 User testing the ModExo workbench (Source: SOUZA, 2018) 45

19 Model of the Muscle-Joint system (Source: SOMMER; FORNER-CORDERO, 2018) 49

20 Experimental setup on a test subject (Source: SOMMER; FORNER-CORDERO, 2018) 51

21 a) Joint angle for the continuous movement with no extra weight, recorded with the IMU; sEMG values for the b) biceps brachii, c) triceps brachii and d) brachioradialis for the continuous movement with no extra weight (Source: SOMMER; FORNER-CORDERO, 2018) 53

22 Estimated elbow angle using the models responses compared to the elbow angle measured with the IMU. The estimated models were ARX, State Space, ARMAX and ARIMAX (Source: SOMMER et al., 2018) 56

23 Comparison between the measured angle of the elbow joint and the angle calculated through the use of the estimated model, for subject 2, with a 1.5kg dumbbell. a) shows the comparison for the continuous movement and b) the comparison for the discrete movement (Source: SOMMER et al., 2018) 57

24 Hammerstein-Wiener model structure (Source: SOMMER; FORNER-CORDERO, 2018) 59

25 Comparison between the measured angle of the elbow joint and the angle calculated through the use of the estimated model, for subject 1, with a 1.5kg dumbbell. a) shows the comparison for the continuous movement and b) the comparison for the intermittent movement (Source: SOMMER; FORNER-CORDERO, 2018) 63

26 Comparison of the estimated and measured joint angle using the same model calculated with the first data set, but using the EMG data from the second test set as input for subject 2 with a 1.5kg dumbbell. a) shows the comparison for the continuous movement and b) the comparison for the discrete movement (Source: SOMMER; FORNER-CORDERO, 2018) . . . 64

27 Comparison between the measured angle of the elbow joint and the angle calculated through the model in real time. a) shows the comparison for no extra weight b) the comparison for 2kg extra weight and c) the comparison for 3kg extra weight . . . 73

28 Acting forces on the base . . . 88

29 Acting forces on the abduction/adduction joint . . . 89

30 Acting forces on the flexion/extension joint . . . 90

31 Numerical simulation of the base . . . 91

32 Numerical simulation of the joint shafts . . . 91

33 Numerical simulation of the cover . . . 92

34 Forces applied to the knee joint . . . 92

35 Numerical simulation of the knee joint . . . 93

36 Diagram showing the exoskeleton block diagram control . . . 95

37 Free body diagram of the exoskeleton . . . 96

38 Position θ_2 versus time for an external load = 0 . . . 101

39 Position θ_2 versus time for an external load = 100 N . . . 101

40 Position θ_2 versus time . . . 102

41 Sliding surface versus time . . . 103

LIST OF TABLES

1 Model orders for each subject (Source: SOMMER et al., 2018) 56

2 Correlation factor and root-mean-square error for the calculated and measured angle values (Source: SOMMER et al., 2018) 58

3 Model orders for each subject (Source: SOMMER; FORNER-CORDERO, 2018) 62

4 Correlation factor, coefficient of determination and root-mean-square error for the calculated and measured angle values (Source: SOMMER; FORNER-CORDERO, 2018) 65

5 Model orders for test subject 72

6 Correlation factor, coefficient of determination and Root-mean-square error for the real time estimated angle values 72

7 Exoskeleton model parameters 96

CONTENTS

Part I: INTRODUCTION **14**

1 Introduction **15**

1.1 Bibliographic Review 15

1.1.1 EMG Control 16

1.1.2 Hybrid Control and Other Control Modalities 23

1.1.2.1 Hybrid Control 23

1.1.2.2 Other Control Modalities 24

1.1.3 State-of-the-Art of Exoskeletons and Exoskeleton Control 25

1.2 Objective 30

2 Methodology **31**

Part II: EXOSKELETON PLATFORMS **34**

3 Trunk and Lower Limb Exoskeleton for Stable Autonomous Walking (ETMICAE) **35**

3.1 Description 35

3.2 Mechanical Structure 35

3.2.1 Hip 37

3.2.2 Knee 38

4 Upper Limb Exoskeleton With One Degree of Freedom (ULEXO) **40**

4.1 Mechanical 40

4.1.1 Structure 40

4.1.2 Actuator 41

4.2 Electronics 41
4.2.1 EMG Sensor 42
4.2.2 Microprocessor 42
4.2.3 Driver 43

5 ModExo 44

5.1 Mechanical 44
5.1.1 Structure 44
5.1.2 Actuator 44
5.2 Electronics 45
5.2.1 Sensors 45
5.2.2 Driver 45
5.2.3 Microprocessors 46
5.3 Discussion 46

Part III: CONTROLLER DESIGN 47

6 Model-based EMG-driven Control 48

6.1 Control Description 48
6.2 Experimental Methods 49
6.2.1 Subjects and experimental setup 50
6.2.2 Experimental Protocol 50
6.2.2.1 Experimental Data Processing 52
6.3 Linear System Model 54
6.3.1 Modeling 54
6.3.2 Results 55
6.4 Non-Linear System Model 58
6.4.1 Modeling 59

6.4.2 Results . . . 62
6.5 Discussion and Conclusions . . . 65

Part IV: TESTING **67**

7 Control Testing **68**

7.1 Calibration . . . 68
7.1.1 Equipment and Materials . . . 68
7.1.1.1 EMG sensor . . . 68
7.1.1.2 Microprocessor . . . 69
7.1.2 Subjects and experimental setup . . . 69
7.1.3 Experimental protocol . . . 70
7.1.4 Experimental data processing . . . 70
7.1.5 Modeling . . . 70
7.2 Testing . . . 71
7.2.1 Data processing . . . 71
7.2.2 Results . . . 72
7.3 Discussion and Conclusions . . . 74

Part V: DISCUSSIONS, CONCLUSIONS AND FUTURE WORK **75**

8 Discussions and Conclusions **76**

9 Future Work **79**

References **81**

Appendix A – ETMICAE Calculations, Simulations and Materials **88**

A.1 Hip . . . 88
A.1.1 Applied Forces . . . 88

A.1.2 Materials . . . 88

A.1.3 Calculations and simulations . . . 89

A.2 Knee . . . 90

A.2.1 Applied forces . . . 90

A.2.2 Materials . . . 93

A.2.3 Calculations and simulations . . . 93

Appendix B – Actuator Control 94

B.1 Exoskeleton Model . . . 94

B.1.1 Exoskeleton . . . 94

B.1.2 Modeling . . . 95

B.2 Control . . . 97

B.2.1 General Characteristics . . . 97

B.2.2 Impedance Control . . . 97

B.2.3 Impedance Control Design . . . 98

B.2.4 Sliding Mode Control Design . . . 99

B.3 Simulation Results . . . 100

B.3.1 Impedance Control . . . 100

B.3.2 Sliding Mode Control . . . 101

B.4 Conclusions . . . 102

Annex A – Sparkfun Muscle Sensor V3 Schematic 104

Annex B – ModExo Control Hardware Schematics 106

PART I

INTRODUCTION

1 INTRODUCTION

In the Introduction it is presented the context and the need for assistive devices along with a bibliographic review. It presents an historical review on the usage of EMG to control prostheses and exoskeletons. As a conclusion the goals of this work are detailed.

1.1 Bibliographic Review

In the United States, the number of people between the age of 18 and 64 that has some kind of movement disability has increased about 12% from 1981 to 2014 (VON-SCHRADER; LEE, 2017). In Brazil, about 13 million people has some kind of motor disability (IBGE, 2012). Two of the main disability causes are stroke and spinal cord injury. Yearly, 15 million people suffer stroke. From these, 5 million are fatal and 5 million cause a permanent disability. These number have been increasing in recent years and studies indicate they will increase even further (MACKAY et al., 2004). From 250 thousand to 500 thousand people suffer spinal cord injury yearly. The three main causes of spinal cord injury are traffic accidents, falls and violence. Moreover, with the rising in life expectancy of the world population (WATKINS, 2005), the number of people affected by disabilities that difficult movement also raised.

Due to these factors, there is a growing need for mechanisms that assist human movements. One of these mechanisms is the robotic exoskeleton.

Robotic exoskeletons are electromechanical structures coupled to the human limbs, capable of doing or assisting movements. A robotic exoskeleton is usually composed of joints and rigid bodies (PONS, 2008). One of the major problems of exoskeletons is the user's intention identification. There are several biological signals that can be used to control an external device. For exoskeleton control, that has the goal of moving a certain limb, it is interesting to use the same signals that are used to control the human motion, like the neural control signals responsible to activate the muscles. Since these signals cannot be accessed directly, the use of electromyography (EMG) has been explored to control these devices.

The surface electromyography (sEMG) signal represents the electrical activity generated by the motor units of the muscles as a response to the activation provided by innervating motor neurons and measured on the skin surface. The information present in the EMG signals is a composition of the synaptic inputs received from the motor neurons and the electrical properties from the muscle fibers (FARINA; MERLETTI; ENOKA, 2014).

There are several other approaches to the control of a mechanical limb apart from the EMG signal. Among the relevant methods, some have been used in combination with EMG for the control of the prostheses or orthoses. These approaches will be described in section 1.2.2.

1.1.1 EMG Control

In 1955, Battye and colleagues (BATTYE; NIGHTINGALE; WHILLIS, 1955) first proposed the use of proportional EMG control. The authors developed an apparatus capable of performing open and close actions so that the test subject could perform a grasping task. The apparatus consisted of electrodes attached to the skin of the forearm, an electrical amplifier, a discriminator, which powered a solenoid when input signal was detected. The solenoid activated a hook, closing it. As a result, the authors were capable of designing a control system sensitive enough to close, and remain closed, when the test subject gripped a pencil in the fingers, regardless of the movement of other limbs. They concluded that the signal captured by the apparatus successfully eliminated the EMG signal from other muscles.

In 1965, Bottomley et al. (BOTTOMLEY, 1965) proposed another method for EMG-driven prostheses control. Two EMG electrode channels were placed on the forearm, one on the hand extensors and another on the hand flexors, to measure the muscle activity. The signal from the muscles were amplified, rectified and smoothed. To remove the "cross-talk", that is, the influence of the neighbor-muscle signals on the targeted muscle signals, the signal of the neighbor muscle was subtracted from the signal obtained from the target muscle. These signals were used to control a Split hook capable of grasping objects, that exerted a force proportional to the EMG signal intensity. To control the desired force, a force sensor was attached to the hook. This device included a feedback control system that was capable of increasing or decreasing the Split hook grasping force based on the measured EMG signal. When the force sensor detected zero force, that is, the hook is not grasping the object anymore and it is freely moving, the intensity of the EMG signal controlled the hook speed. A backlash generator was introduced in the electrical system to attenuate random variations around a preset threshold, that widens as the force feedback signal increases. The authors state that, after a few minutes wearing the apparatus, all the test subjects, even amputees, were able to control the hook in a graded manner (BOTTOMLEY, 1965).

Also in the sixties of the last century, Alter (ALTER, 1966) designed an exoskeleton control using two differential electrodes, one on the biceps and one on the triceps. Both signals were rectified and then the triceps signal was subtracted from the biceps signal and fed to an adjustable low-pass filter. This signal was used as input signal to a power amplifier driving an electric motor. Strain gauges were attached to the exoskeleton to measure the force measurement, and this signal entered the system as a feedback signal.

In 1966, Isidori and Nicolo (ISIDORI; NICOLO, 1966) first described the myopulse processing technique, which was later developed by Childress et al. (CHILDRESS; HOLMES; BILLOCK, 1971) and Philipson (PHILIPSON, 1985). The myopulse processor works as follows: when the absolute value of the EMG exceeds a predetermined threshold value, the processor output is turned on. When the EMG activity increases, the duty cycle of the myoprocessor output also increases. An illustration of this method can be seen in figure 1.

In this system, two sets of electrodes were placed over the targeted muscle where the detection of electrical signal was desired. The EMG signal was sent to the myopulse processor, where the input signal was amplified and transformed into Pulse Width Modulated (PWM) signal. This PWM signal was sent to the microcomputer. Then, the microcomputer processed the PWM signals and sent the output signals to control the prosthetic arm according to the control algorithm. The myopulse processor is an electrical circuit composed of a dual comparator, with the value of the resistors defining the threshold value δ.

The EMG signal is analog, since it is a measure of the electrical activity of the muscle. To use this signal in a digital controller it should be digitized. However, a major advantage of the myopulse processor is that there is no need for a conventional analog-to-digital converter. The author also implemented a classification method for the control of a prosthesis. Differently from the previous control methods, where the joint actuation was proportional to the intensity of EMG signal, this system can perform different movements. In this work, by measuring the intensity of EMG signals from two electrode sets, the author

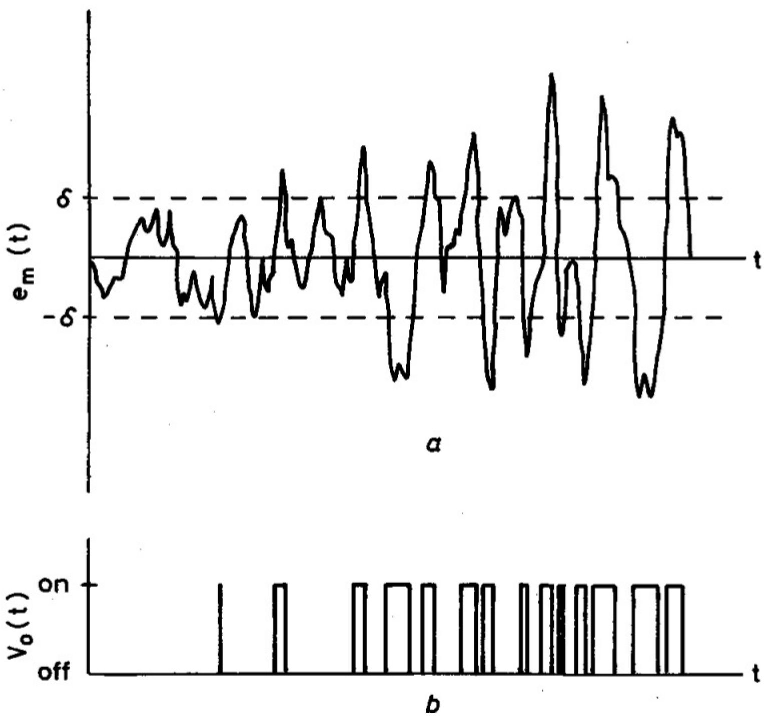

Figure 1: Illustration of the myopulse processing technique. The upper trace shows a typical bandpass-filtered EMG signal recorded with surface electrodes. The output will remain off as long as the absolute value of the EMG signal in the upper trace is below the level δ, otherwise the output will be turned on. The lower trace illustrates the output from the myopulse processor (Source: PHILIPSON, 1985) .

was able to control seven different states. Figure 2 shows the proposed dynamic area for the prostheses control. Considering the intensity of the input from the two target muscles one of the seven possible states is performed, according to the corresponding area on the dynamic area (PHILIPSON, 1985). This control system was applied to a prostheses and tested on four amputee volunteers. With proper training sessions, the volunteers were able to perform some daily tasks such as grasping a plastic cup containing water, pouring the desired amount and then releasing the cup. In the case of the non-amputees, the subjects could achieve good control over the seven-state control system.

In 1977, Parker et al. (PARKER; STULLER; SCOTT, 1977) sought to develop a EMG signal processor for a prosthesis with a minimal error in the identification of the desired action. The authors developed a model that extracts the relevant information from the myoelectric signal obtained by a bipolar electrode configuration. One of the main strengths of this model is that the pooled motor unit firing rate reflects the contraction level and is thus the information parameter in the myoelectric signal. In 1980, Hogan (HOGAN; MANN, 1980a, 1980b), also in search of a better myoprocessor, developed a similar mathematical model to estimate muscle force based on EMG signal.

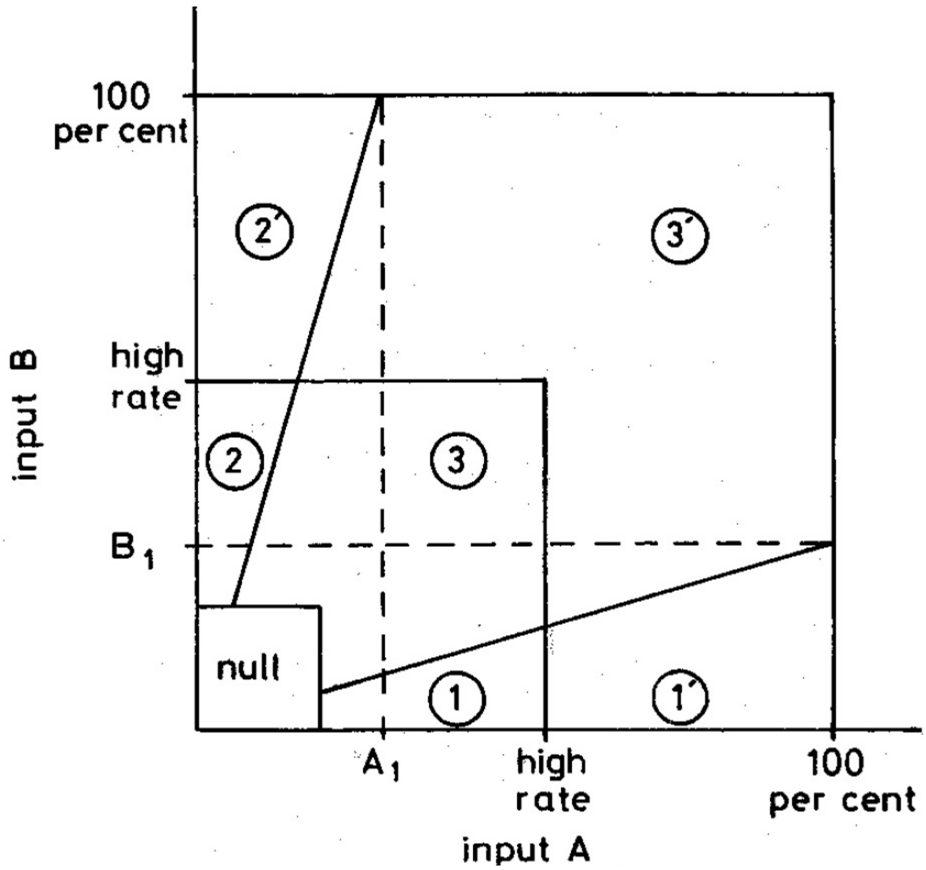

Figure 2: Diagram showing the possible movement areas according to the muscle inputs (Source: PHILIPSON, 1985) .

The myoelectric signal can be modeled as a zero-mean stochastic process. In order to estimate the user's control signal, it is necessary to add a nonlinearity to the estimator. Typically, a full-wave rectifier is used for this nonlinearity, followed by a low-pass filter. Evans et al. (EVANS et al., 1984) proposed another model based approach to this EMG control problem. The authors used a logarithmic nonlinearity, followed by a a linear minimum mean-square error in the EMG-force estimation. In this way a Kalman filter was inserted to estimate the control signal.

Hudgins (HUDGINS; PARKER; SCOTT, 1993) proposed a control strategy for a multifunction prosthesis based on the classification of myoelectric patterns into different movements. Initially, the author conducted tests on both healthy subjects and amputees. The test consisted of an isometric and isotonic contraction and a contraction (e.g. flexion, extension, etc.) with no constraints related to force, velocity or range. The subjects were asked only to make consistent motions, starting from a comfortable neutral position.

By taking the average of the EMG signal for the first 300ms to 600ms of the movement, that is the onset, it was possible to detect different signal patterns for each movement, shown in figure 3. Other control schemes, based on steady state levels, are limited to only three limb functions: for an elbow mechanism, one can only control extension, flexion and the off-state. The scheme proposed by Hudgins targets the EMG signal of only one muscle and is capable of assigning as many functions as the number of distinct signal patterns generated by the muscle.

Since the prosthesis is capable of performing different movements, it is necessary to implement a classifier that chooses the desired movement or action based on the input signal. An Artificial Neural Network (ANN) was chosen as the classifier. The authors proposed a group of parameters, called features, which served as input to the classifier. The following features were chosen to represent the myoelectric patterns: Mean Absolute Value (MAV): it is the mean value of the rectified signal throughout the data segment; Mean Absolute Value Slope: is the difference, in value, between the MAV of each segment; Zero Crossing (ZC): number of times the waveform crosses the zero value (a "dead-zone" must be introduced to avoid noise inducted zero crossings); Slope Sign Changes (SSN): the number of times the slope of the waveform changes sign (the same "dead-zone" applied previously must be applied here); Waveform Length (WL): is the cumulative length of the waveform throughout the data segment. By using these previous features, one can get values for waveform amplitude, frequency and duration. This classification method has become known as the Time Domain feature set (NIELSEN et al., 2009).

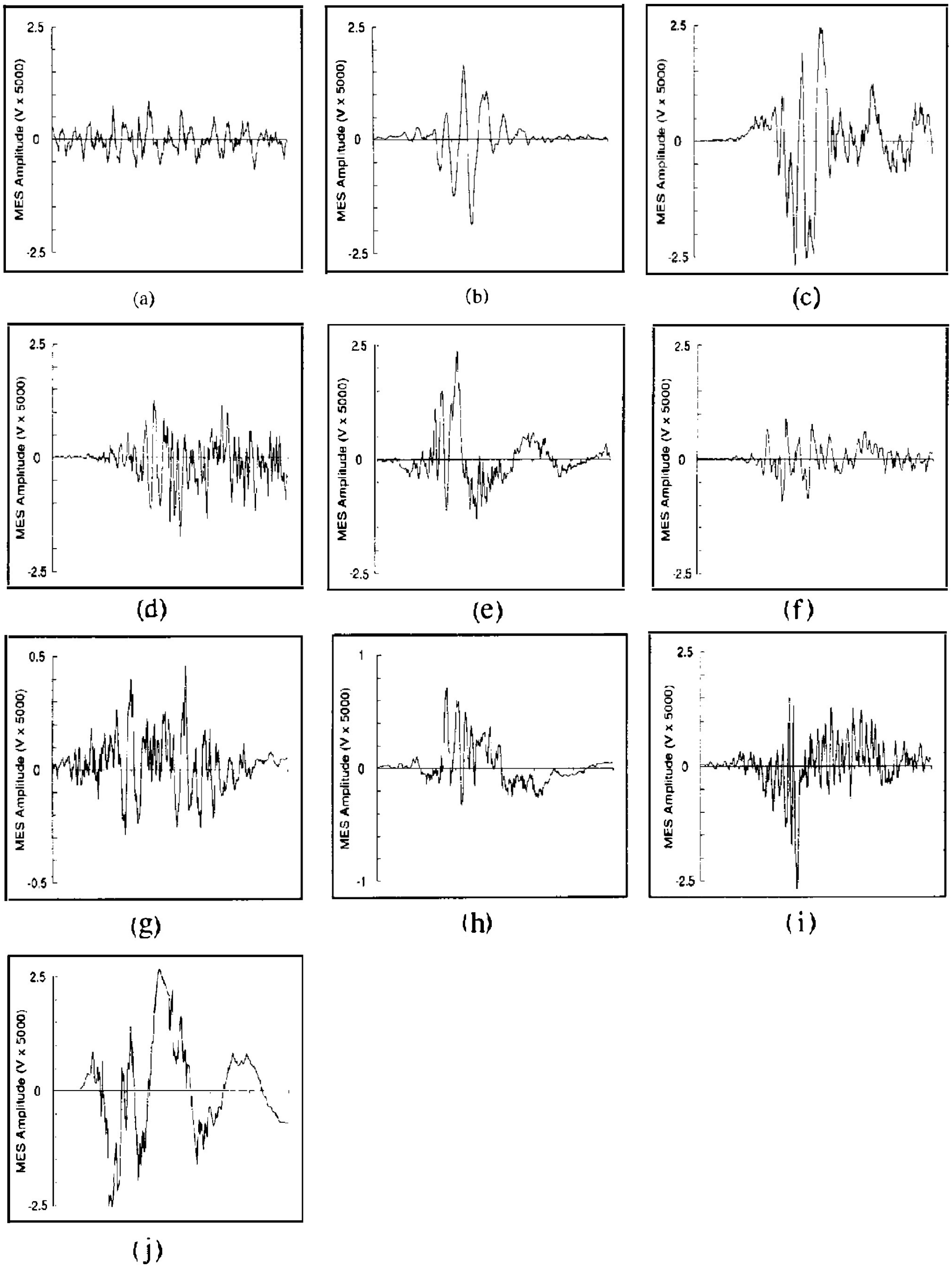

Figure 3: Average of the first 300ms of the EMG recordings for the following movements: For a healthy subject: a) Isometric contraction; b) elbow flexion; c) Forearm supination; d) elbow extension; e) wrist flexion; f) forearm pronation; for the amputee subject: g) inward humeral rotation; h) contraction of the flexor muscle group; i) contraction of the extensor muscle group and j) biceps/triceps co-contraction (Adapted from HUDGINS; PARKER; SCOTT, 1993).

The tests showed that the subjects were capable of performing up to four different movements with an accuracy ranging from 70-95%, before training. However, a major drawback from this control scheme is that, since the classification method only considers the movement onset, the EMG signal must always start from a resting position. If the user tries to switch from one movement to another in a period of time smaller then the averaging window (300ms-600ms), the control scheme will fail.

Englehart (ENGLEHART et al., 1999), further developing the pattern recognition problem, tested some time-frequency-domain sets for the EMG signal processing. The sets used were: Short-time Fourier Transform (STFT), Wavelet Transform (WT) and Wavelet Packet transform (WPT).

The same group also proposed a method to overcome the previous problem regarding the fast transition between two different movements (ENGLEHART; HUDGINS, 2003). To do so, instead of segmenting the EMG data into multiple frames for classification, now the data was acquired continuously on a single, unsegmented window. In this scenario, the data acquired from 12 subjects were compared using the Time Domain statistics and using the time-frequency-domain sets. The Time Domain sets outperformed the time-frequency-domain sets in continuous data acquisition.

Jiang (JIANG; ENGLEHART; PARKER, 2009) proposed a method to estimate force from the Mean Square Value (MSV) of the EMG signal. MSV is defined as the mean value of the square of the signal throughout the data segment. By stating that it is possible to maintain the muscle cross-talk at low levels, it is possible to determine a direct relationship between muscle force and sEMG measurements.

In 2013, Aung, Al-Jumaily (AUNG; AL-JUMAILY, 2013) proposed a method to estimate an upper limb joint angle using a back propagation neural network (BPNN) integrated into a Virtual Human Model (VHM). EMG data from anterior deltoid, posterior deltoid, biceps brachii and triceps brachii were recorded and used as input to the model. The applied neural network was composed of three layers: input layer, using the EMG signal from the four arm muscles; hidden layer using Levenberg-Marquadt algorithm; and, finally, the output layer.

In 2016, Rahmatian et al. (RAHMATIAN; MAHJOOB; HANACHI, 2016), using a Support Vector Machine (SVM) algorithm associated with a Time-Delayed Artificial Neural Network (TDANN), proposed a method for continuous estimation of ankle joint angle. The authors used sEMG data from tibialis anterior, gastrocnemius medialis and gastrocnemius lateralis muscles. The SVM algorithm was used for classification of sEMG while the TDANN approximated angles and velocities of the ankle joint. The authors achieved an accuracy of 95.4% for the classification procedure.

Also in 2016, Mamikoglu et al. (MAMIKOGLU et al., 2016) proposed a method to estimate ankle joint angles based on muscle modeling and the measurement of EMG signals. The model is based on a multiple input, single output (MISO) Autoregressive Integrated Moving-Average with Exogenous Input (ARIMAX) model, using integrated EMG measurements as input and estimating the corresponding joint angles. The proposed method was capable of achieving fitness values above 0.9 for single speed contractions and above 0.77 for varying speed contractions.

The addition of a load can decrease the accuracy of EMG-based control systems up to 60% (AL-TIMEMY et al., 2013). To address this problem, in 2017, Azadet et al. (AZAB; ARVANCH; MIHAYLOVA, 2017) acquired EMG data from three subjects, using four different loads and used them for training a k-Nearest Neighbors algorithm (KNN) and Naive Bayes classifiers (NB). The results showed mean accuracy of 53% and 36%, for KNN and NB respectively, for subject-dependent conditions, and 22% and 36% for subject-independent conditions.

1.1.2 Hybrid Control and Other Control Modalities

Hybrid control refers to a group of controllers that combine the information from different sources in order to perform the control of the mechanism.

1.1.2.1 Hybrid Control

If the subject had some residual shoulder movement it is possible to combine a joystick at the shoulder with EMG for a movement classification method (LOSIER; ENGLEHART; HUDGINS, 2007). The system was capable of performing nine different activities. Eight of then were controlled by the position of the shoulder and one by EMG input when the user performed a humeral rotation movement. The Time Domain technique was used to differentiate the EMG readings from humeral rotation from the normal shoulder movements.

Fougner and Stadvahl (FOUGNER et al., 2008; STAVDAHL et al., 2011) used force sensors on the EMG electrodes to measure external forces. This application is useful for the cancellation of artifacts caused by these forces (e.g. movement artifacts).

Fougner (FOUGNER et al., 2011) noted that different limb positions associated with daily activities can affect the EMG signal results. To overcome this problem, the EMG signal was associated with accelerometers placed at the user's forearm and biceps. This allows the pattern recognition system to know the position and orientation of the limb, compensating for eventual changes on the EMG signal.

1.1.2.2 Other Control Modalities

If EMG sensors are difficult to place or if they cause discomfort to the user other techniques such as Mechanomyography (MMG) may be used. Mechanomyography is the measurement of the mechanical vibrations caused by the contraction of the muscle. In Silva (SILVA; CHAU; GOLDENBERG, 2003), the MMG sensors were used as a substitute of the EMG sensors, when the EMG sensors are of difficult placement or unconfortable for the patient. This method can also be referred as phonomyogram, vibromyogram, soundmyogram or acoustomyogram, since the sensor is composed of an accelerometer and a microphone that detects the air vibration between the sensor and the target muscle.

Kenney (KENNEY et al., 1999) used the dimensional change of the muscle as control signal for his control strategy. This technique is called Myokinemetric. The author designed a sensor, composed by a Hall Effect sensor and a permanent magnet. The relative distance between these two components varied according to the dimensional change of the subject's muscle. To validate this strategy a tracking test was performed, where the test subject was supposed to track a signal presented on a screen by controlling the dimensions of his muscle.

Stadvahl (STAVDAHL; GRONNINGSAETER; E.MALVIG, 1997) used ultrasound to estimate the muscle force. As the muscle contracts, the shape of the muscle changes. The ultrasound, when transmitted to a medium, generates an echo signal that can be acquired with a sensor. Using this information, a relation between ultrasound and force signals can be determined by the Cross Correlation technique. Chen (CHEN; CHEN; DAN, 2011) attached ultrasound transducers to the subject's forearm to estimate the wrist angle using the ultrasound signal.

Nightingale (NIGHTINGALE, 1985) used force and slip sensors on the Southampton Hand to detect forces applied to the hand and relative slipping motion between the hand and objects. By using the force and slip sensors paired with an EMG control, a state machine controller was implemented. According to the EMG signal magnitude the control logic would open or close the hand and by using force sensor measurements, more specific states for the hand movement, like holding or squeezing an object were accessed.

1.1.3 State-of-the-Art of Exoskeletons and Exoskeleton Control

The exoskeletons can be grouped as a function of their applications: performance enhancement, haptic interfaces, remote operation, functional assistance (active orthoses and prostheses), rehabilitation and motor control exploration. In this work two groups will be focused on: the performance enhancement and the functional assistance. The performance enhancement exoskeleton allows healthy users to perform a difficult task by either reducing the forces or the expended energy, or perform a task that is impossible to accomplish by human strength or skill, solely. The functional assistance assists the user by modifying or recovering the motor function of the neuromuscular and skeletal system. However, this distinction, in some cases, can be not as clear (DOLLAR; HERR, 2008).

One of the major incentives to the development of exoskeleton has been the Exoskeletons for Human Performance Augmentation (EHPA), a program supported by the Defense Advanced Project Agency (DARPA), an agency of the United States Department of Defense. This program is developing exoskeletons capable of increasing the capabilities of ground soldiers beyond that of a human. There are three critical technologies that are the focus of this program: Energy, power and actuation; controls and haptic interface; design and integration (GARCIA; SATER; MAIN, 2002).

HAL (Hybrid Assistive Limb) is an exoskeleton focused on both performance-augmenting as well as rehabilitation (SANKAI, 2011). The HAL-5 is a full-body exoskeleton. The joints are powered by DC motors with harmonic drives placed directly on the joints. The exoskeleton is attached to the user by harnesses at the hip, thighs, calves, upper arms and forearms, as well as the shoe that is equipped with ground reaction force sensors.¡.

The HAL-5 utilizes a broad range of sensors for its controller. The intention detection is done primarily by sEMG sensors. As soon as the EMG level exceeds a threshold, the motion support is triggered. An assistive torque is provided to the user. This torque is composed of three parts: an assistive torque; a viscous torque that prevents high velocities, maintaining safety; and a gravity compensating torque (KAWAMOTO et al., 2010). In some experiments, the motion intention detection was done by the ground reaction sensor, to adapt the exoskeleton for patients with spinal cord injury. When the user shifts its weight to the next stance leg, the reaction force on this leg is higher than the other, triggering the exoskeleton motion (TSUKAHARA et al., 2015). Also, there are potentiometers, gyroscopes and accelerometers for the measurement of the angle, speed and acceleration of limbs and joints.

In (OTSUKA et al., 2011) the authors further developed the HAL upper-limb ex-

Figure 4: HAL-5 exoskeleton (Source: SANKAI, 2011) .

oskeleton for meal assistance. It is composed of a shoulder joint with three degrees of freedom and an elbow joint with one degree of freedom. Also, a grasp assistance mechanism is attached to the forearm to allow for manipulation of objects by the user.

One interesting aspect of the HAL exoskeleton is its modularity. Currently, there are separated products for upper-limbs, lower-limbs, lumbar support, as well as other modalities, like a heavy-duty and a disaster recovery exoskeleton (CYBERDYNE, 2007).

The manufacturer states that the full-body HAL-5 weighs approximately 23kg, has a continuous operating time of approximately 2 hours and 40 minutes and is capable of lifting objects up to 70kg. The HAL® exoskeleton is capable of performing different activities such as standing up from a chair, walking and climbing up and down stairs.

The HAL® exoskeleton is already used in many medical institutions in Japan and already received certification for clinical use in Europe. It is commercialized by Cyberdyne Inc.

The Berkeley Lower Extremity Exoskeleton (BLEEX), funded by the DARPA, is a self-powered exoskeleton that enhances the strength and endurance of a human (KAZEROONI, 2006).

The BLEEX exoskeleton has 7 degrees of freedom (DOF) per leg: 3 DOF at the hip, 1 DOF at the knee and 3 DOF at the ankle. For the hip, both the flexion/extension and

Figure 5: University of California at Berkeley's BLEEX exoskeleton (Source: ZOSS; KAZEROONI; CHU, 2006) .

the abduction/adduction joints are aligned to the human joint, but the rotation joint is positioned behind the user and under the torso. The reason is that an aligned rotation joint would result in limited ranges of motion and singularities in some of the human postures. For the ankle, the flexion/extension axis coincides with the human ankle joint, but the abduction/adduction and rotation axes do not coincide with the human joint axes and form a plane outside of the human's foot. However, the forefoot is compliant, allowing the toe flexion. The exoskeleton is only rigidly connected to the user at the hip and the foot (ZOSS; KAZEROONI; CHU, 2006).

The BLEEX structure and actuation was designed based on the clinical gait analysis (CGA) of an 75-kg person. Analyzing the CGA, it was possible to determine which exoskeleton joint required actuation, based on the joint torque and power during gait. From this analysis, it was determined that the flexion/extension joints of hip, knee and ankle and the abduction/adduction joint of the hip should be actuated.

Initially, the selected actuator for the BLEEX was a double-acting linear hydraulic actuators. These actuators are compact in size, low weight and capable of exerting high forces. They are placed in a triangular disposition in relation to the joint, resulting in a torque that varies according to the joint angle (CHU; KAZEROONI; ZOSS, 2005).

The average power consumption of the BLEEX during the walking cycle is 1143 W, compared to 165 W of mechanical power exerted by the human during normal gait. This exoskeleton is capable of supporting up to 75 kg and walk at speeds up to 1.3 m/s.

In a later study, the feasibility of using electrical motors instead of the previous hydraulic ones was analyzed. The designed electrical motors weighed an average of 4.1 kg opposed to the 2.1 kg hydraulic actuators. While the electric actuator weight is all centered in the actual joint, about 40% of the weight hydraulic actuator is located away from the joint. At test performed at ground-level walking at the speed of 1.3 m/s, it was measured that the actuator power consumption was 598 W. Comparing both actuators, the electrical actuator is 95% heavier and 92% more power efficient (ZOSS; KAZEROONI, 2006).

An hybrid Hydraulic-Electric Power unit (HEPU) was designed in the attempt to provide autonomous energy for the exoskeleton. The hydraulic energy would supply the necessary mechanical parts of the exoskeleton, while the electrical energy would power the computer, sensors and other peripherals. Even though the designed HEPU could provide the necessary requirements of electrical and hydraulic power, it exceeded in both weight and noise output. The desired weight and noise output were 23 kg and 78 dBA, respectively. The achieved values were 30 kg and 87 dBA (AMUNDSON et al., 2006).

The control of the BLEEX exoskeleton has no sensors attached to the user. Every sensor is located only on the exoskeleton. It uses the forces applied by the environment and the user to the exoskeleton as the control signal (STEGER; KIM; KAZEROONI, 2006). The inverse dynamics of the exoskeleton is used as a feedback so that, when accounting for the user force, the control loop gain approaches an unitary value. This control strategy has two main advantages: it allows for wide bandwidth maneuvers, necessary since the exoskeleton needs to respond to a wide variety of the human's movements; it is independent to changes in the user dynamics. The trade-off of this control strategy is that it needs an accurate model of the exoskeleton dynamics. To address this, experiments in (GHAN; KAZEROONI, 2006) applied system identification methods to calculate the exoskeleton dynamics.

One of the most well-established exoskeletons for disabled users is the ReWalk™. The ReWalk™ is a lower extremity, battery powered exoskeleton that allows individuals with thoracic or lower level motor complete spinal cord injury to walk independently. It is suitable for adults who have preserved bilateral upper extremity function. The user must be using crutches to maintain balance. The mechanical structure is composed of bilateral supports parallel to the thighs and legs, articulated at the knee and hip. A rigid shoe insert fixes the user's feet. Velcro closures distributed at the legs and thighs and a waist belt secure the attachment between user and exoskeleton. The computer-based controller and the batteries are stored within a backpack. A tilt sensor is placed at the exoskeleton structure, near the waist (ESQUENAZI, 2013).

The active joints of the ReWalk^{TM} are the knee and waist joint. The ankle joint is passive joint with spring-assisted dorsiflexion. The exoskeleton has five different operation modes: walk, sit-stand, stand-sit, up steps and down steps. In the 'walk' mode, the stepping procedure is triggered by the forward flexion of the upper body, measured by the tilt sensor. The maximum walking velocity is 2.2 km/h. The mode selection can be made through an user-operated wrist pad. There is also the option to manually control the position of the lower limbs (ZEILIG et al., 2012).

Figure 6: The ReWalk^{TM} exoskeleton worn by an user and its basic structure (Source: ESQUENAZI, 2013) .

Some studies have been performed with the ReWalk^{TM} (ZEILIG et al., 2012; FINEBERG et al., 2013; TALATY; ESQUENAZI; BRICENO, 2013). Overall, the participants of the test were satisfied with the device, being able to walk without falling. The volunteers reached the level of being able to walk 100m with the use of crutches. However, they have not attained proficiency to use the device on a daily basis. It is stated that the users found relative difficulty with wearing and adjusting the device.

Even tough many advancements in this area have been made, the effective use of an exoskeleton continues to be extremely difficult. Even though many technologies have been advertised lately, there is a lack of quantitative studies available to researchers (YOUNG; FERRIS, 2017).

The MIT exoskeleton, a quasi passive exoskeleton concept, explores the passive dynamics of human walking trying to achieve a lighter and more efficient exoskeleton. The tests showed that the total metabolic cost of walking increased when used the exoskeleton while carrying a load, compared to no exoskeleton being used while carrying the load in a backpack. The increase in metabolic cost was found to be 10% higher (WALSH; ENDO; HERR, 2007). Nevertheless, the participants in the tests stated that carrying the load while wearing the exoskeleton was more comfortable compared to carrying the backpack alone (VALIENTE, August, 2005). Another study demonstrated the exoskeleton is capable of transferring up to 90% of the load to the ground, depending on the gait phase, but increases the metabolic cost in a range from 32% up to 74%, depending on some variations of the mechanical structure and actuation of the exoskeleton (WALSH, February, 2006).

It has been previously studied that one of the major problems of ambulation devices for paraplegics is the high-energy demands imposed to the user. Franceschini et al. (FRANCESCHINI et al., 1997) conducted a survey on patients that utilized reciprocating orthoses (ARGO, RGO, HGO). From the 74 patients, 24 patients abandoned the use of the mechanism by the end of the study. One of the main reasons was the excessive energy cost.

1.2 Objective

The objective of this dissertation is to design the controller of a one-degree-of-freedom exoskeleton using sEMG signals from the user as the input signals. The controller must be accurate in replicating the movement desired by the user, as well as requiring little training from the user.

2 METHODOLOGY

The ideal control method would be one that requires no prior training. The user would be capable of controlling the mechanism as easily as he can control his own limb. Of course this is an ideal scenario and, as stated in many previous studies already cited in this work, we are still far from understanding the real dynamics of limbs, muscles and electromyography signals.

With those challenges in mind, how can we design a control that is capable of controlling a mechanical "limb-like" mechanism?

One potential idea is to design a control method that mimics the physical characteristics of the human limb, that is, a biomimetic control. Biomimetics is the study of biological mechanisms and processes with the purpose of synthesizing similar products and behaviors by an artificial mechanism which mimics natural ones (MERRIAMWEBSTERDICTIONARY, 2009). To achieve this biomimetic behavior, the model-based control method can be a great candidate.

Biomechatronics, control designing and system modeling must be combined to achieve an EMG-Driven exoskeleton controller that is both safe and natural to user. Therefore, it is necessary to approach this design in a structured manner.

First, available and in development exoskeleton platforms at the Biomechatronics Laboratory at Escola Politécnica of the University of São Paulo (USP) will be analyzed in respect to its mechanical and electronic design, as well as its sensoring, to better determine the one that is more appropriate for the application of the EMG-driven controller.

An experimental procedure will be conducted to obtain EMG and angle data of a predetermined movement, for the design of the controller.

Two different EMG-to-Angle model estimation methods will be applied and evaluated: a linear method and a nonlinear method. They will serve as a base for the controller design. The methods will be compared according to their accuracy, complexity and applicability in the chosen exoskeleton platform.

The controller will be adapted so it can be applied in real time conditions. The controller undergoes testing in real time conditions to determine if the goals proposed for this work were achieved.

Finally, the results are discussed and compared to similar works from the literature.

Figure 7 presents a diagram with this structure in a visual manner.

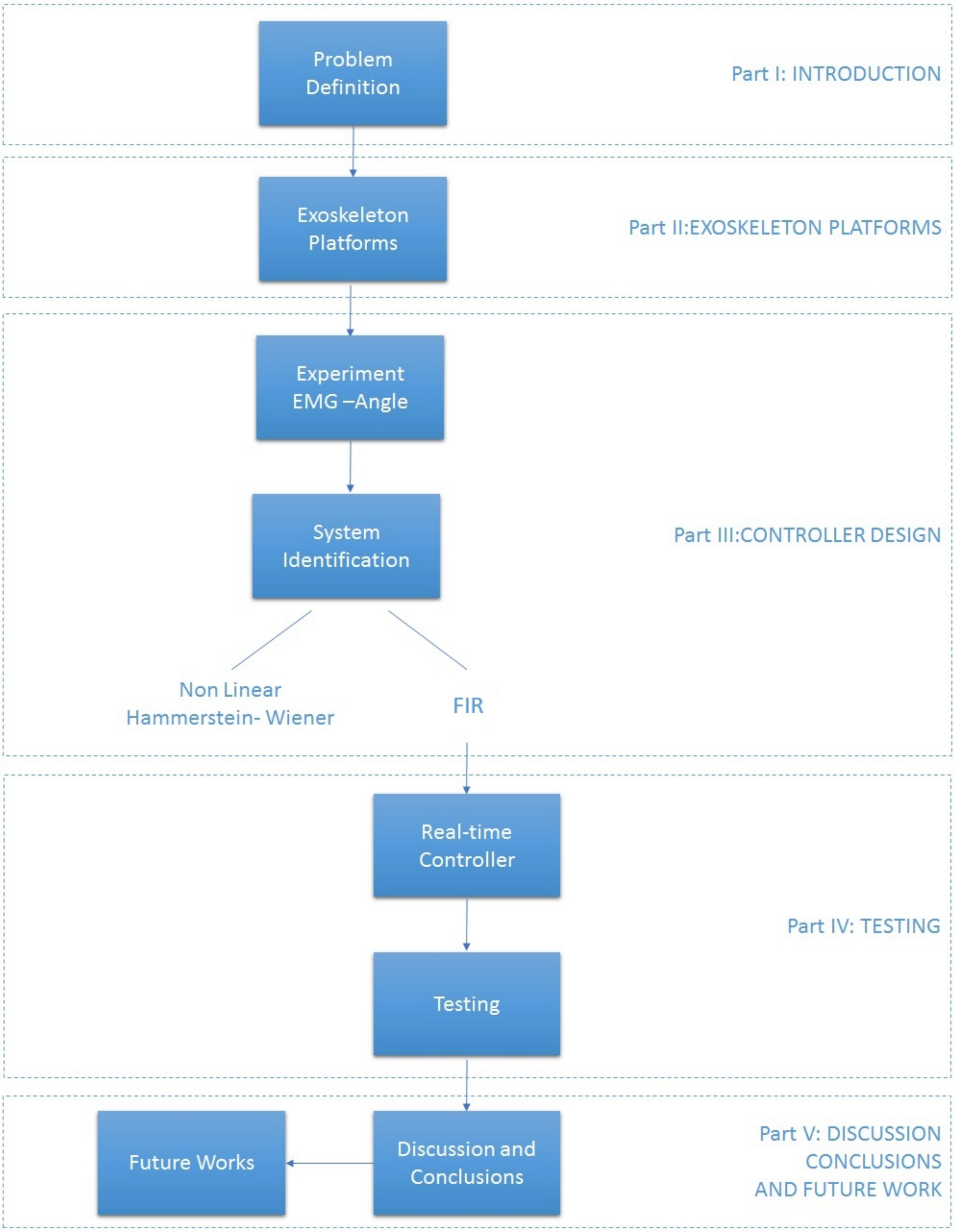

Figure 7: Visual representation of framework/methodology

PART II

EXOSKELETON PLATFORMS

In this part, it is described exoskeletons available and being developed at the Biomechatronics laboratory that can be used to implement the control strategies developed in this work

3 TRUNK AND LOWER LIMB EXOSKELETON FOR STABLE AUTONOMOUS WALKING (ETMICAE)

3.1 Description

The ETMICAE is a bipedal trunk and lower limb exoskeleton to assist the walking movement of people with motor disabilities. It allows the use of the exoskeleton by people that cannot maintain a full control of their body and lower limbs. It includes human gait stability control.

It is currently being developed at the Biomechatronics Laboratory - Mechanical Engineering and Mechanical Systems Department - Escola Politécnica of the University of São Paulo (USP). This project is being developed in collaboration with the Rehabilitation Medicine Institute of the Clinics Hospital - Medicine School of USP, São Carlos School of Engineering (EESC-USP).

When the project is completed, it will mainly contribute in two major areas: Clinical studies and technological studies. For clinical studies, the ETMICAE will be transferred to a clinic to test and evaluate the exoskeleton on subjects with motor disabilities. For the technological studies, the exoskeleton will act as platform for testing of mechanical, electrical and control technologies developed at the Biomechatronics laboratory.

3.2 Mechanical Structure

With the goal of using ETMICAE as a platform to test the sEMG controllers, the author of this dissertation was responsible in designing the hip, thigh, knee and leg mechanical structure, as well as its coupling components. The 3D modeling of the exoskeleton can be seen in figure 8. The explanation of this design is described in this section. Calculations for the mechanical design are described in Appendix A.

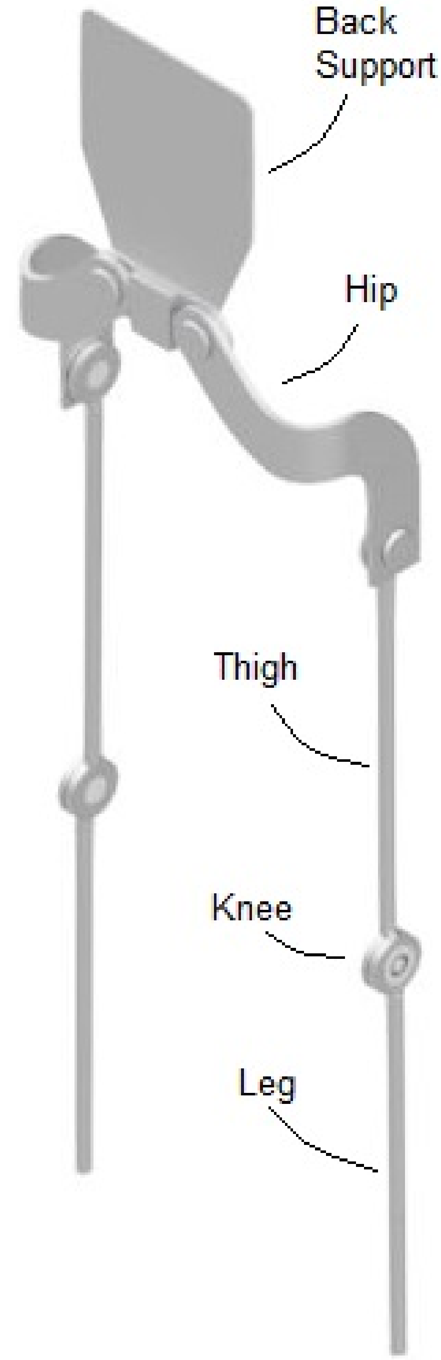

Figure 8: Assemble of the ETMICAE

3.2.1 Hip

The hip of the exoskeleton will have four degrees of freedom, being the abduction/adduction and flexion/extension of both thighs. The exoskeleton will not have the pronation/supination movement of the thighs.

The hips are composed of the following parts:

A base will will attach the hip of the exoskeleton to the support of the motors, located at the back of the user.

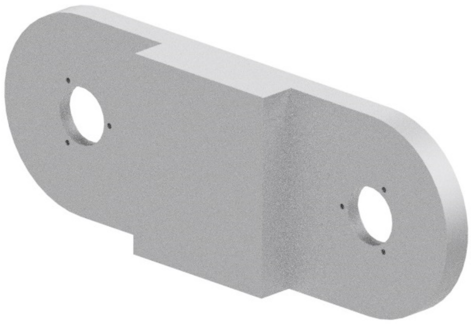

Figure 9: Base

Attached to the base there are two joints that will perform the abduction/adduction degree of freedom for the thighs. For this coupling a shaft supported by two ball bearings will allow the relative movement between the two parts. Between the thigh component and the base, a low friction thrust washer is inserted to support the axial forces and allow smooth slipping. Another thrust washer is positioned at the external part of the joint to, in conjunction with an aluminum cover, support the axial forces.

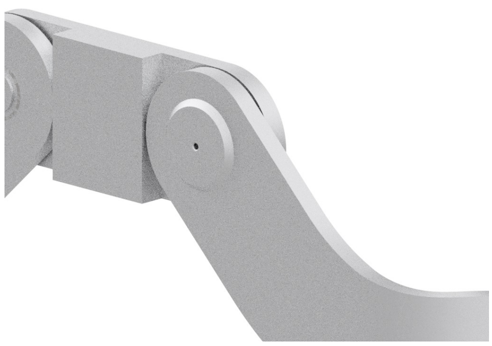

Figure 10: Hip abduction/adduction joint

Linked to these joint, a folded aluminum plate extends to the next hip joint.

The lateral joint allows for the flexion/extension degree of freedom of the thighs. This joint is also composed by a shaft supported by two ball bearings with a thrust washer

Figure 11: Hip plate

between the two parts.

Figure 12: Hip flexion/extension joint

3.2.2 Knee

Each knee will have only one degree of freedom, aligned to the flexion/extension joint of the user. It is constituted of the following parts:

A bar that extends from the flexion/extension joint of the hip to the knee joint. This bar stays parallel to the user's thigh.

Attached to the thigh bar, a rotation joint allows the flexion/extension movement of the mechanism. At this joint a shaft supported by two ball bearings will be used. Between the two parts of the joint a low friction coefficient thrust washer is positioned to support

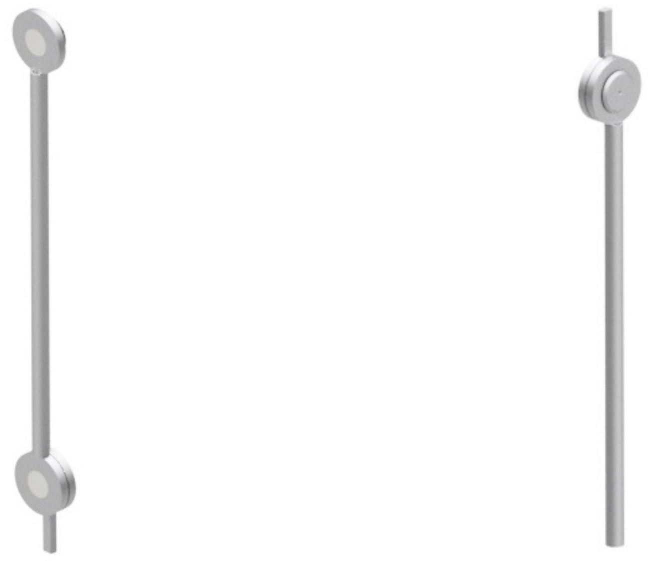

(a) Thigh (b) Leg

Figure 13: Thigh and leg bars

the axial forces and allow for smooth sliding between the parts. Another thrust washer is positioned at the external part of the joint, along with a metallic cover, to support the axial forces.

Figure 14: Knee flexion/extension joint

Attached to this joint, another metallic bar extends to the ankle.

4 UPPER LIMB EXOSKELETON WITH ONE DEGREE OF FREEDOM (ULEXO)

This chapter briefly describes an upper limb exoskeleton with one degree of freedom already available at the Biomechatronics laboratory. This system was first designed in (SOMMER, 2015).

4.1 Mechanical

4.1.1 Structure

The exoskeleton structure is made of aluminum bars. The aluminum structure is attached to a Power Window Lifter steel mechanism.

The user's arm is placed at the aluminum structure and held firmly through the use of rubber straps.

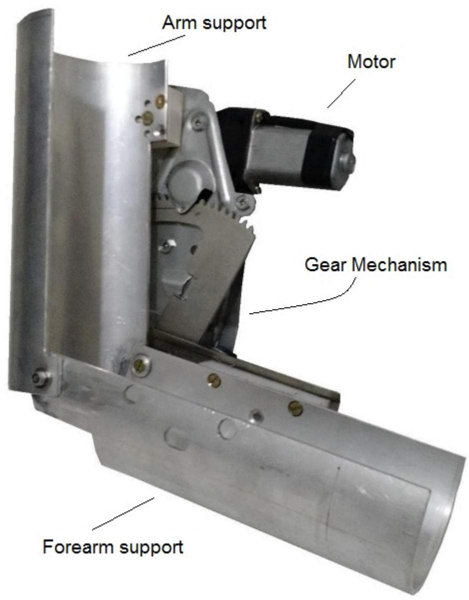

Figure 15: Upper limb exoskeleton with one degree of freedom (Source: SOMMER, 2015)
.

4.1.2 Actuator

The actuator of the exoskeleton is composed by a (578VA, Mabuchi Motor Co., ltd., Japan) DC motor and a Power Window Lifter mechanism.

This DC Motor was chosen because of its high power-to-weight ratio, low dimensions and low price.

In order to increase the motor torque, the DC motor is attached to a modified Power Window Lifter, a mechanism with gear coupling with a reduction factor of 10:1. Modeling, Impedance Control and Sliding Mode Control studies have been conducted with this exoskeleton and are presented in Appendix B

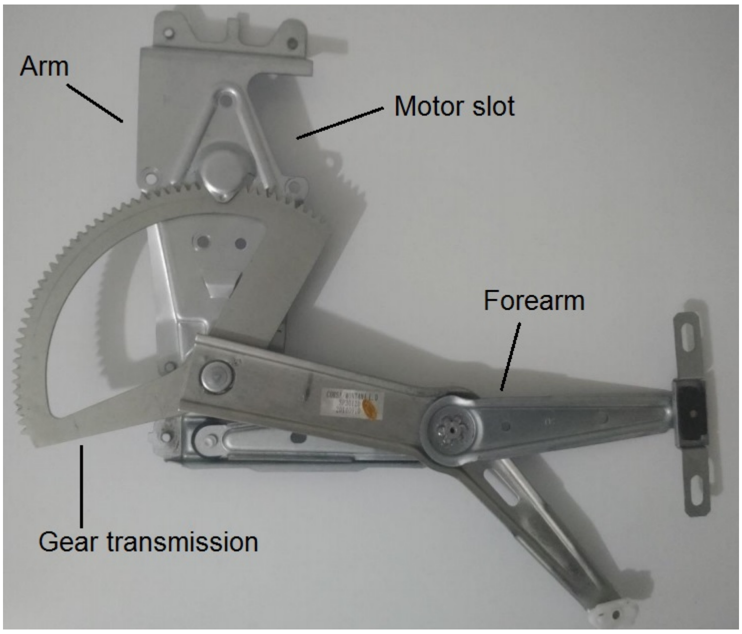

Figure 16: Power Window Lifter (Source: SOMMER, 2015) .

4.2 Electronics

The electronics system of the exoskeleton is composed of the following parts: An sEMG sensor, that acquires the sEMG signal of the biceps muscle; a microprocessor to process the analog sEMG signal, apply the control logic and output a PWM signal; a motor driver that receives the PWM signal as input and outputs the necessary power to drive the DC motor.

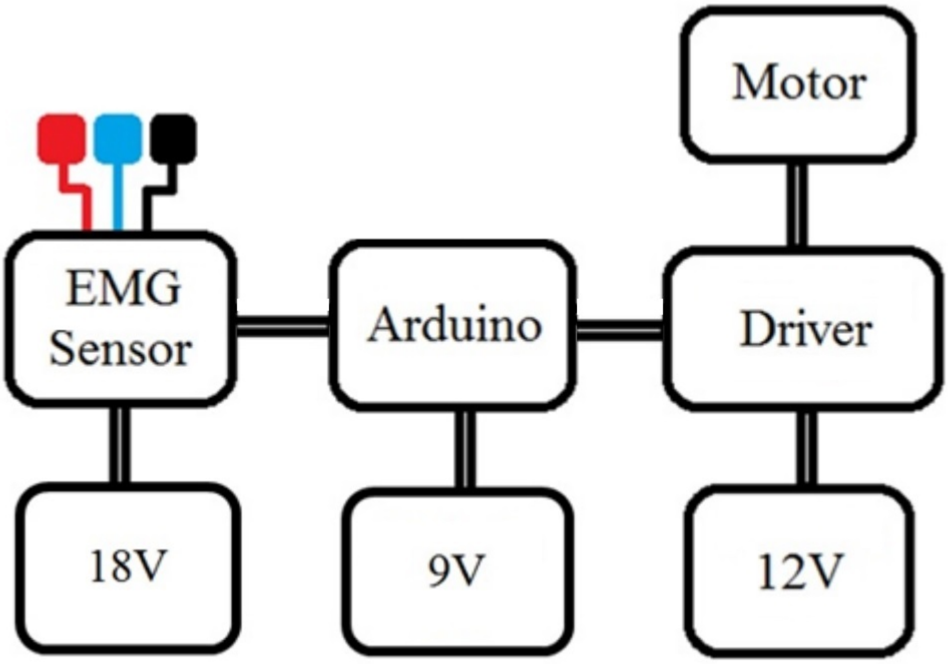

Figure 17: Schematic of the electronics (Source: SOMMER, 2015) .

4.2.1 EMG Sensor

The EMG Sensor is (Muscle Sensor V3, Sparkfun Electronics®, USA).

Three electrodes are attached to this sensor: Two electrodes are placed at the target muscle and measure the difference of electrical activity and one is placed at an electrically neutral region of the body, like a bony area, and serves as the ground signal.

The signal from the electrodes is differentially amplified in the AD8221 amplifier; then, the signal is amplified twice by TL084 operational amplifiers; the signal is rectified using 1N4148 diodes; the rectified signal is attenuated by a filter with 2Hz cutoff frequency; at last, the signal is amplified with an adjustable gain.

The Sensor output is sent directly to the microprocessor.

4.2.2 Microprocessor

The microprocessor is an (Arduino UNO, Arduino, S.r.l., Italy). It was chosen for its low cost, ease-of-use, extensive available documentation and easy communication to the Muscle Sensor V3. It has a built-in 10-bit resolution Analog/Digital converter and is capable of emitting PWM signals. Also, it is possible to connect more sensors to this microprocessor, for future adaptations of the exoskeleton.

4.2.3 Driver

The DC motor demands electrical currents up to 24A. Motor Drivers for 12V, 24A DC motors are expensive. For this reason, a motor driver was designed for the specific use on this exoskeleton.

The driver has two inputs (clockwise rotation and counter-clockwise rotation) that receives the PWM signal from the microprocessor for the desired direction of motion. There are two outputs that are connected to each one of the motor electrical terminals.

The driver is composed of a H-Bridge of MOSFETs. The chosen components were IRF4905 for P channel and IRLB3813 for N channel. The gate of the P channel MOSFET is powered by a TIP122 transistor.

To avoid the situation where every MOSFET of the H-Bridge is activated at the same time, which would cause a short circuit between the poles of the battery, a protection circuit was implemented. The protection circuit is composed of 74LS08 AND gates and 74LS04 NOT gates. In case both the inputs are powered, no signal reaches the gates of transistors, protecting the circuit.

This exoskeleton has some limitations, since it does not contain angular sensors, has limited speed control and requires extensive work for a feedback controller to be implemented.

5 MODEXO

This chapter briefly describes a development platform for exoskeleton research available at the Biomechatronics laboratory. The system was first presented in (SOUZA, 2018)

5.1 Mechanical

5.1.1 Structure

The ModExo is an exoskeleton development platform. It replicates one degree-of-freedom of an exoskeleton, coupling a motor to a load cell.

A load cell is attached to the structure of the exoskeleton segment, which provides contact torque between user and exoskeleton (SOUIT, 2016).

The load cell is designed to deform elastically in a Wheatstone bridge configuration and measured the force applied to the exoskeleton.

A 3D printed case protects the strain gauges wiring and serves as an attachment to a forearm support.

The ModExo is assembled in a wooden portable case. The assembly can be seen in figure 18.

5.1.2 Actuator

The actuator of the ModExo is composed of a flat brushless DC motor (EC90 Flat, Maxon Motors AG, Switzerland). It has integrated an encoder (Encoder MILE, Maxon Motors AG, Switzerland), and a harmonic reduction (Harmonic Drive 100:1, Harmonic Drive, Ltd, Japan)).

The motor was chosen for its high torque-velocity curve. It also offers high power-

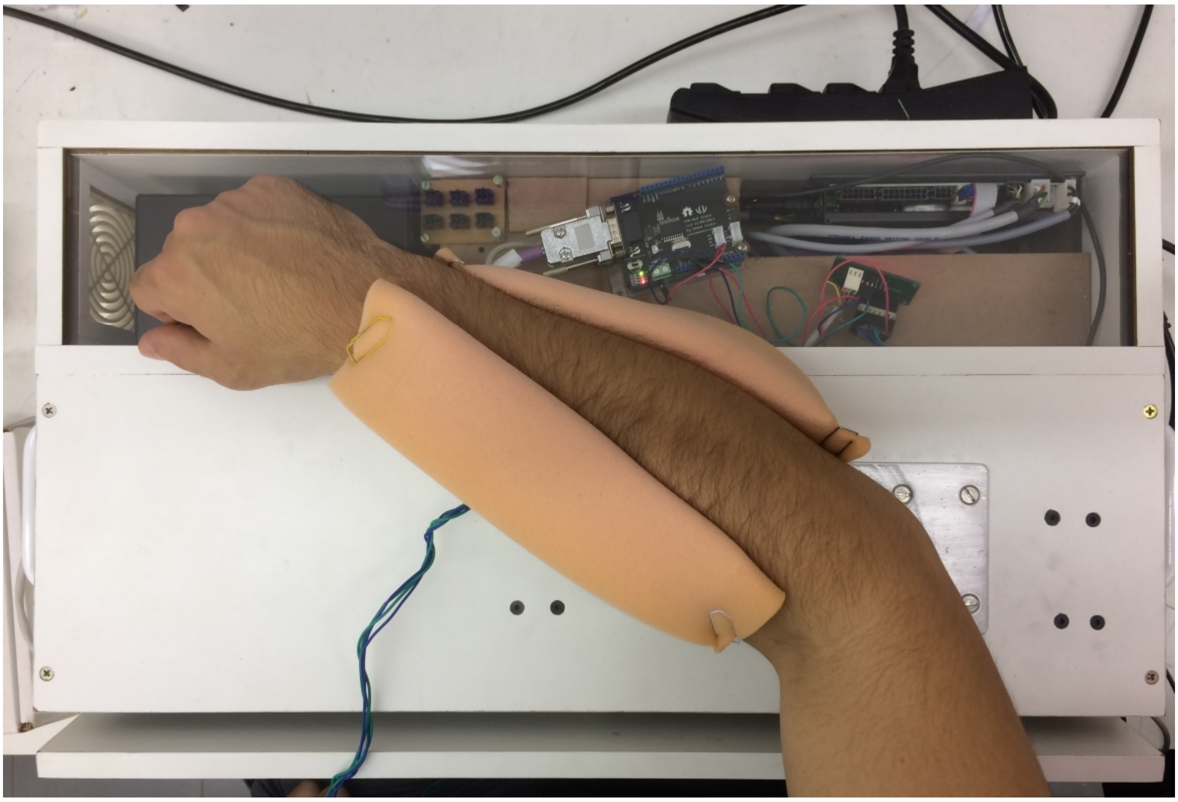

Figure 18: User testing the ModExo workbench (Source: SOUZA, 2018) .

to-mass ratio and has low dimensions. Because of its flat design, it reduces the torsional deflection of the motor when placed in parallel with the human body.

5.2 Electronics

5.2.1 Sensors

Strain gauges, assembled in full Wheatstone bridge, attached to the load cell, provide contact torque information.

5.2.2 Driver

The driver used is also from Maxon (EPOS2 70/10, Maxon Motors AG, Switzerland). It receives position commands from the central controller and transmits them to the Maxon motor. It also receives position feedback from the encoder integrated to the motor.

5.2.3 Microprocessors

A microcontroller based on the (Arduino UNO, Arduino, S.r.l., Italy) acts as a high level controller, implementing the impedance control and position output for the Maxon motor.

A CAN bus shield (CAN bus Shield, Seedstudio, China) is used as a CAN bus interface, managing communication between the the microcontroller, EPOS driver and amplification board. It is connected to the microcontroller as a shield.

5.3 Discussion

The ModExo can be used as a platform that imitates the elbow joint in an upper limb exoskeleton. Since it has position sensors already implemented, an easy-to-use communication between a personal computer and the platform, and the possibility to implement different control methods, it is the best candidate between the three exoskeleton platforms, to implement the control method designed is this work.

With the exoskeleton platform determined, it is necessary to design the controller for EMG-to-Angle relation. In the next chapter, the controller design is described.

PART III

CONTROLLER DESIGN

In this part, control methods for the EMG are proposed and designed to be implemented in an exoskeleton platform.

6 MODEL-BASED EMG-DRIVEN CONTROL

The content of this section is an extended version of two full papers presented at IEEE Conferences: EMBC 2018 and BioRob2018 (SOMMER et al., 2018) and (SOMMER; FORNER-CORDERO, 2018).

There are different electrophysiological signals that can be used to control an exoskeleton. Therefore, it seems interesting to use the control signals that are used by the body to activate the muscles. As these neural control signals are not easily accessible, surface electromyography has been used as a control signal for upper-limb exoskeletons (LENZI et al., 2012).

6.1 Control Description

The Model-Based control method utilizes a dynamic model of the body to predict the dynamic response according to the input given to the model. There are basically three types of dynamic models: mathematical, system identification and artificial intelligence models (ANAM; AL-JUMAILY, 2012).

For this work it was chosen the system identification modeling approach. It is often used because of the difficulty in describing the dynamic model with mathematical equations. To do so, a set of inputs and outputs are measured experimentally and then an identification algorithm develops the relationship between the system inputs and outputs. There are certain assumptions needed to use these models, such as linearity/non-linearity, model structure and model order.

By using a dynamic model that mimics the user's limb dynamics, the exoskeleton will be capable of performing limb-like movements using the sEMG signals as input. A mathematical system modeling should consider the EMG to muscle force generation and, afterwards, take into account the different muscle forces around a certain joint along with the corresponding moment arms and inertial parameters of the segments to obtain the angle, as shown in figure 19.

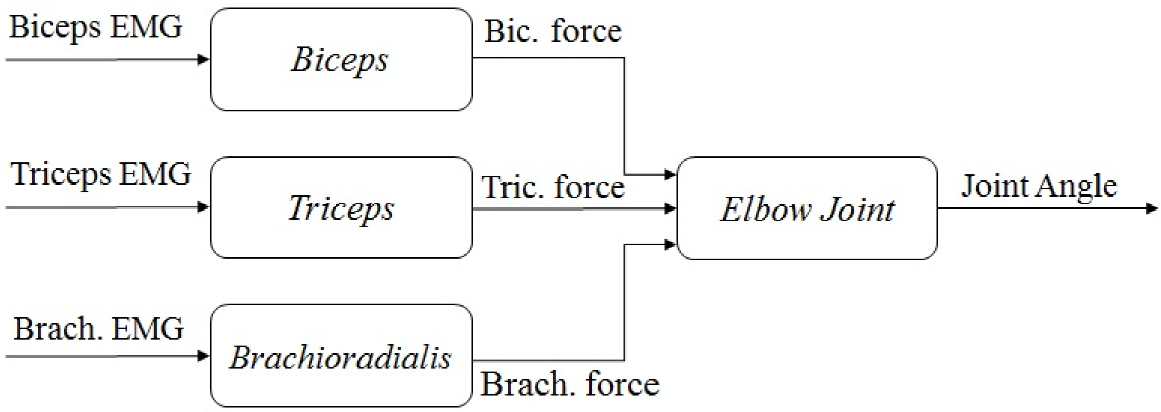

Figure 19: Model of the Muscle-Joint system (Source: SOMMER; FORNER-CORDERO, 2018) .

It is important to note that human models are complex and nonlinear (KATO et al., 2015). One considerable advantage of using system identification as estimation technique is that it is possible to model the system as a black box. This allows the model estimation to be calculated without precise knowledge about muscles and joint dynamics (ABBASI-ASL et al., 2011).

The main disadvantage of this control method is that, in order to develop the dynamic model, experiments must be conducted on each subject to calculate his/her specific model parameters. Differences between testing sessions, such as the electrode positioning on the subjects' skin can alter the results from the controller. This may require a calibration procedure to readapt the controller to the new conditions.

6.2 Experimental Methods

This section presents a method to estimate the elbow joint angle from surface electromyography (sEMG) measurements of biceps, triceps and brachioradialis. This estimation is of major importance for the design of human robot interfaces based on sEMG, for the modeling of the muscular system and for the design of bio-inspired mechanisms. However, the interpretation and processing of electromyography signals is challenging due to nonlinearities, unmodeled muscle dynamics noise and interferences. In order to determine an estimated model and a calibration procedure for the model parameters, a set of experiments were carried out with six subjects. The experiments consisted of series of continuous (cyclical) and discrete elbow flexo-extensions. The sEMG data from the biceps brachii, triceps brachii and brachioradialis and the joint angle were recorded. After the model was selected, a second experiment was performed in order to validate the estimation procedure. The results show an effective model for the EMG-to-angle relation with great values for both correlation and root-mean-square error when compared to the measured angle data.

The experimental procedures involving human subjects described in this work were approved by the Comitê de Ética em Pesquisa do Hospital Universitário da Universidade de São Paulo (CEP-HU/USP).

6.2.1 Subjects and experimental setup

Six volunteers (age: 34.3 ± 14.7 years, height: 1.74 ± 0.1 m, weight: 67.9 ± 15.7 kg, 4 male, 2 female, all right-handed) with no known neuromuscular deficit participated in the experiments. Elbow joint angle along with the surface electromyography (sEMG) of three right arm muscles, biceps brachii, triceps brachii and brachioradialis were recorded. sEMG was measured with 3 pairs of (FREEEMG 1000, BTS Bioengineering Corp., Italy) electrodes with an electrode separation of 20mm with the electrode diameter being 4mm. A pair of electrodes was placed on the biceps and other pair on the triceps following the SENIAM guidelines (SENIAM, 2004). To determine the electrode positioning for the brachioradialis muscle, the subject was asked to apply force to flex the forearm while keeping it at 90°. Then, the electrode was placed on the belly of the muscle and its respective pair placed distally at a 20mm following the muscle fiber direction. The sampling rate was of 1kHz with 16 bit resolution. The user interface was the BTS FREEEMG software (BTS, Spa, Italy).

To measure the joint angle, a six degrees of freedom Inertial Measurement Unit (IMU, VN-100 from VectorNav®, TX, USA), with 0.01° precision, was attached on the internal aspect of the forearm, located at two-thirds distance from the elbow to the wrist. The angle values were acquired with a rate of 100 samples per second. The data were collected with Matlab® (The MAthworks Inc, MA, USA) using a dedicated library provided by the inertial sensor manufacturer.

The experimental setup can be seen in figure 20.

6.2.2 Experimental Protocol

The subject sat on a chair, with the knees flexed at 90°, the back perpendicular to the ground with the scapulas pressed against the wall. The back of the arm was leaning

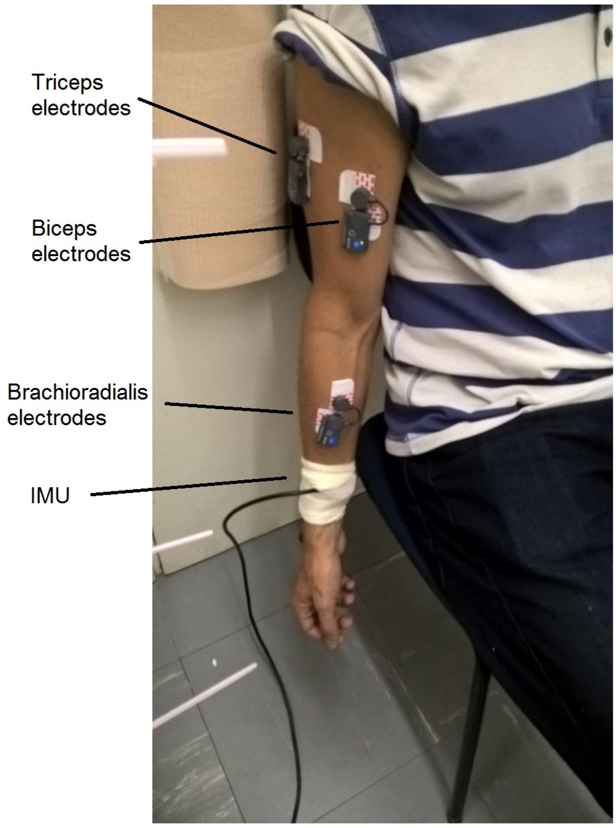

Figure 20: Experimental setup on a test subject (Source: SOMMER; FORNER-CORDERO, 2018) .

against a rubber support that was attached to the wall. This setup guaranteed that the subject was comfortable enough to perform repeated elbow flexions and extensions while maintaining the upper arm steady.

The experimental protocol had three parts: The first one consisted of an isometric force test to obtain the Maximum Voluntary Contraction (MVC). The elbow of subject was kept in a fixed position at 90° and he/she was asked to apply the maximal possible force to flex the elbow. The subject was given a three minute interval before the next set.

In the second part, the subject was asked to perform five consecutive elbow flexion and extension movements from 50° to 140° with a frequency of 0.5Hz, that is, five movements in ten seconds. To help the subject reach the correct target angles a template was attached to the wall parallel to the subject, to provide visual guidance. To achieve the desired movement speed a metronome was set at the speed of 60 BPM so that the subject could synchronize the movements with the sound of the metronome. A minute of rest was given to the subject before the next part.

In the third part the subject was instructed to make an elbow flexion for 1 second, hold his forearm at 140° for 1 s, then a 1 s extension movement and then hold the forearm at 50° for another 1 s. This cycle should be repeated five times. Another one minute resting time was given to the subject. Both of the continuous and interval tests were repeated with 1.5kg and 3kg extra weight placed at the subject's hand.

No subjects reported fatigue during the experiment.

The test was repeated in a different day, on all test subjects to further analyze the repeatability of the model proposed in this work.

All the data from the tests were transferred to Matlab® (The Mathworks Inc, USA). for further analysis and processing.

6.2.2.1 Experimental Data Processing

The EMG data were processed as follows. Further explanations can be found on the literature (ROSE, 2011; HAYASHIBE; GUIRAUD; POIGNET, 2009)

1. high-pass filtering of the EMG data, using a 2nd order Butterworth filter, with a cutoff frequency of 30 Hz, thus removing movement artifact.
2. Wave rectification
3. Second Order low-pass Butterworth Filter, with 1Hz cutoff frequency.
4. normalization with the peak of MVC

This way, the EMG is smoothed and presented as a percentage of the subject MVC instead of Volts.

A low-pass, 20 Hz cutoff frequency, second-order Butterworth filter is applied to the angular data to remove errors and other undesired signals.

Since the position tracking data was sampled at 100 Hz while the EMG data was sampled at 1KHz, all the position tracking data was resampled to 1000 Hz.

Figure 21 shows an example of the recorded elbow angle and processed sEMG for the continuous movement with no extra weight.

Both the angular data as well as the EMG envelope had to be detrended for the models estimation.

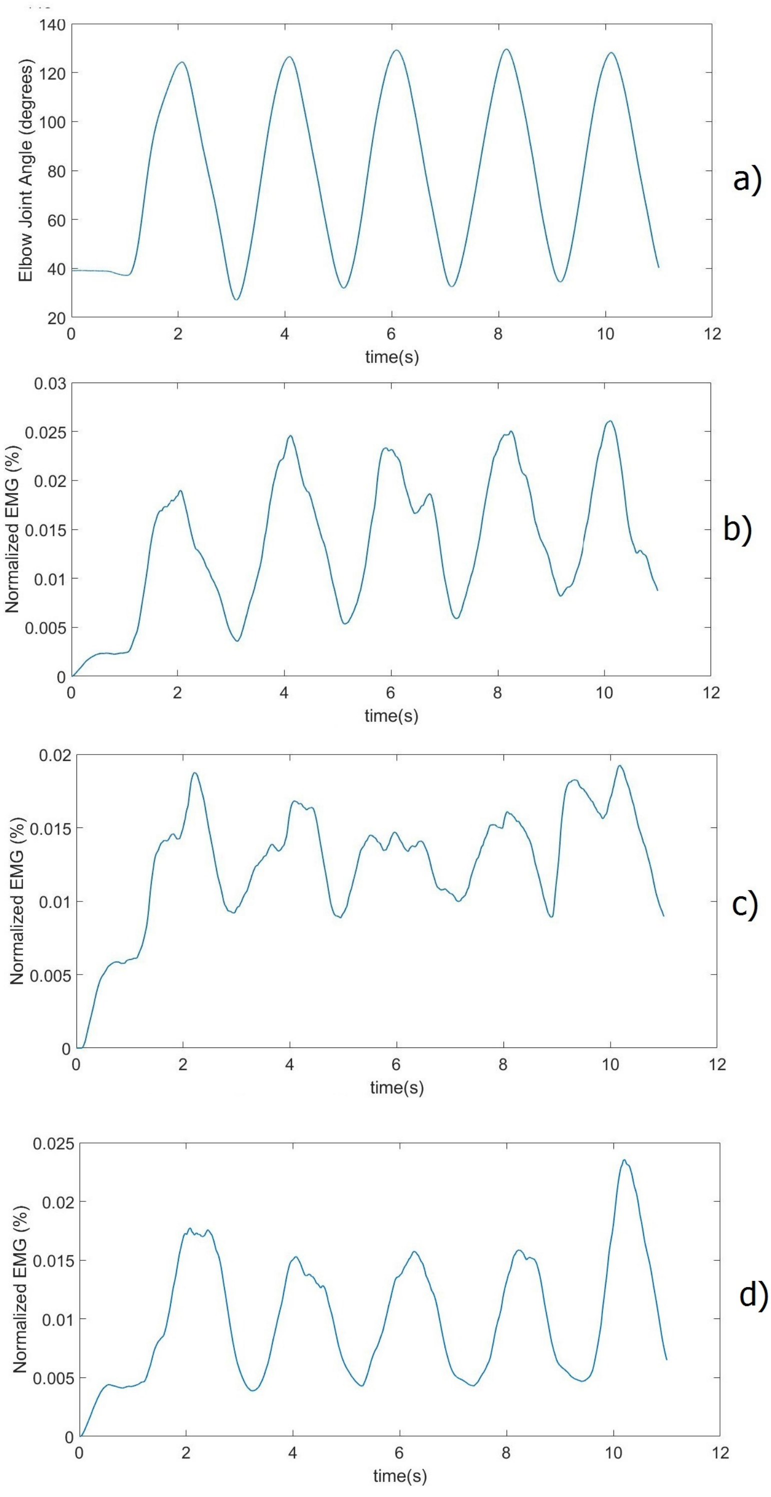

Figure 21: a) Joint angle for the continuous movement with no extra weight, recorded with the IMU; sEMG values for the b) biceps brachii, c) triceps brachii and d) brachioradialis for the continuous movement with no extra weight (Source: SOMMER; FORNER-CORDERO, 2018) .

6.3 Linear System Model

The content of this section has been published in (SOMMER et al., 2018).

6.3.1 Modeling

It was assumed that the arm has the same model with different inertia parameters for the different weights attached to the arm of the subject arm. Considering a simple model of the elbow (arm with only 1 degree of freedom):

$$T = (J + M \cdot L^2) \cdot \ddot{\theta} + B \cdot \dot{\theta} + (m \cdot l + M \cdot L) \cdot g \cdot cos(\theta) \tag{6.1}$$

Where T is the elbow joint torque, J is the forearm inertia, B is the damping factor of the joint, m is the forearm mass, M is the dumbbell's mass, g is the acceleration due to gravity force and θ is the joint angle. From this simple model it is easy to infer that, by changing the dumbbell's mass, the arm model parameters also change.

Four different modeling techniques were applied to determine which one best estimated the model that provides the elbow angle as an output taking the three EMG signals as inputs. These modeling techniques were: Auto-Regressive with Exogenous Input (ARX), Auto-Regressive Moving-Average with Exogenous Input (ARMAX), Auto-Regressive Integrated Moving-Average with Exogenous Input (ARIMAX) and State Space (SS).

ARX and ARMAX are reduced forms of the ARIMAX model. The ARIMAX model can be described using equation 6.2 (MATHWORKS, 2015):

$$A(q)\hat{y}(t) = \sum_{m=1}^{3} B_m(q)u_m(t - n_{k_m}) + \frac{C_m(q)}{(1 - q^{-1})}e(t) \tag{6.2}$$

Where $\hat{y}(t)$ is the output at time t, angle of the elbow joint, in this case; u(t) are the inputs, being the processed sEMG values from biceps brachii, brachioradialis and triceps brachii; e(t) is the white-noise disturbance; n_k is the delay for each input; q is the delay operator; m equals 1 for the biceps EMG signal, 2 for the triceps EMG signal and 3 for the brachioradialis EMG signal; A, B and C are the model parameters, defined by:

$$A(q) = 1 + a_1 q^{-1} + \cdots + a_{n_a} q^{-n_a} \tag{6.3}$$

$$B(q) = 1 + b_1 q^{-1} + \cdots + b_{n_b} q^{-n_b+1} \tag{6.4}$$

$$C(q) = 1 + c_1 q^{-1} + \cdots + c_{n_c} q^{-n_c} \tag{6.5}$$

Where n_a is the number of poles of the system; n_b is the number of zeros plus one and n_c is the number of coefficients of the moving average.

In order to find a solution a hard search was done using 1000 models of each type with random model orders ranging from 1 to 10. A data window of 6s was used to calibrate the model, while the entire data vector was used to validate the model.

Each model was compared to the reference angle using equation 6.6. The orders of the model that achieved the highest fitness value were chosen and are presented at table 1. The parameters of the models were estimated using time-domain data in Matlab® (The Mathworks Inc, USA).

$$Fit = \sqrt{\frac{\prod_{i=1}^{3} \prod_{j=1}^{2} Corr_{ij}}{\prod_{i=1}^{3} \prod_{j=1}^{2} RMSE_{ij}}} \tag{6.6}$$

Where $Corr_{ij}$ is the correlation between the measured angle and estimated angle for each test; $RMSE_{ij}$ is the root-mean-square error (RMSE) between the measured angle and estimated angle (see eq. 6.7); i equals 1 for the 0kg test, 2 for the 1.5kg test and 3 for the 3kg test; j equals 1 for the continuous test and 2 for the intermittent test.

$$RMSE = \sqrt{mean((y - \hat{y})^2)} \tag{6.7}$$

Where y is the measured angle and $\hat{y}$ is the estimated angle.

6.3.2 Results

Figure 22 compares the different models with measured elbow angle and shows the fitness value for each data set.

The ARX model outperforms the other models for every subject and every test set. For this reason it was the chosen model for the subsequent estimation procedures.

The model orders calculated are presented in table 1.

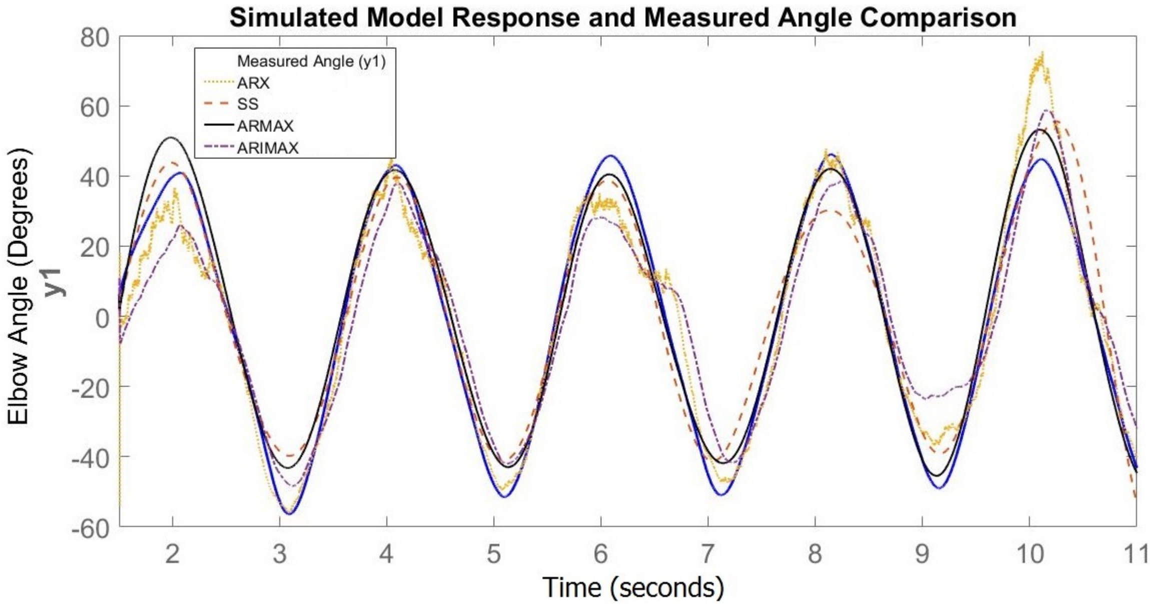

Figure 22: Estimated elbow angle using the models responses compared to the elbow angle measured with the IMU. The estimated models were ARX, State Space, ARMAX and ARIMAX (Source: SOMMER et al., 2018) .

The best model is a model with a null value on the auto-regressive part of the equation. For that reason, the best model is, in fact, a Finite Impulse Response (FIR) model, that can be considered as a particular case of the ARIMAX model.

The FIR model has the following form, as seen in equation 6.8:

$$\hat{y}(t) = \sum_{m=1}^{3} B_m(q)u_m(t - n_{k_m}) + e(t) \tag{6.8}$$

Table 1: Model orders for each subject (Source: SOMMER et al., 2018) .

	n_a	n_b	n_k
Subject 1	0	8, 2, 2	1, 2, 2
Subject 2	0	9, 5, 10	1, 3, 0
Subject 3	0	1, 4, 8	5, 0, 1
Subject 4	0	8, 8, 1	0, 0, 8
Subject 5	0	5, 1, 9	2, 8, 0
Subject 6	0	4, 3, 10	3, 0, 0

Using the values from table 1 as the FIR model orders, it was possible to calculate the model for elbow joint angle using the three sEMG measurements as input and compare it to the experimentally measured values. As an example, figure 23 shows a comparison between the calculated and estimated angle, for continuous and intermittent movement.

Using the same model parameters previously calculated, we estimated the response

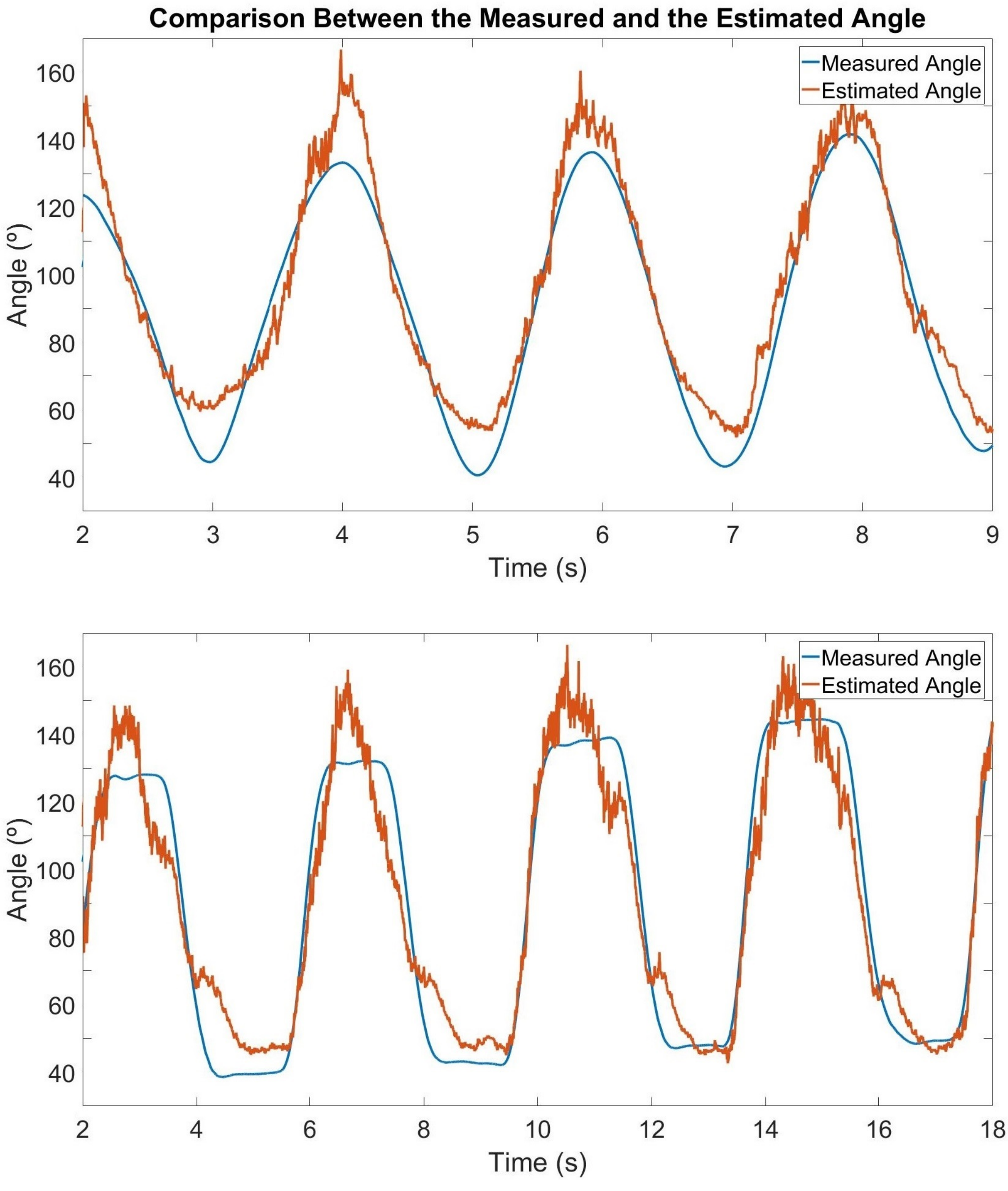

a)

b)

Figure 23: Comparison between the measured angle of the elbow joint and the angle calculated through the use of the estimated model, for subject 2, with a 1.5kg dumbbell. a) shows the comparison for the continuous movement and b) the comparison for the discrete movement (Source: SOMMER et al., 2018) .

Table 2: Correlation factor and root-mean-square error for the calculated and measured angle values (Source: SOMMER et al., 2018)

		Model Estimation, first test set				Same model, second test set				New model, same orders, second test set			
		Continuous		Intermittent		Continuous		Intermittent		Continuous		Intermittent	
		Correlation	RMSE (degrees)	Correlation	RMSE (degrees)	Correlation	RMSE (degrees)	Correlation	RMSE (degrees)	Correlation	RMSE (degrees)	Correlation	RMSE (degrees)
	0 kg	0.9477	13.73	0.9404	17.36	0.0224	65.02	0.1546	60.29	0.9500	10.84	0.8195	20.76
Subject 1	1.5 kg	0.9615	13.21	0.8042	24.30	0.8067	17.06	0.7250	18.50	0.9458	7.959	0.7118	18.79
	3 kg	0.9764	12.30	0.8994	18.10	0.9322	17.23	0.8624	16.80	0.9381	12.64	0.8454	14.47
	0 kg	0.9163	14.32	0.9070	17.27	0.8113	32.33	0.9089	21.53	0.9543	11.59	0.9251	13.64
Subject 2	1.5 kg	0.9707	9.715	0.9585	11.50	0.7685	23.11	0.8647	18.06	0.9544	12.20	0.9062	14.65
	3 kg	0.9329	18.56	0.9494	12.83	0.8715	21.50	0.9419	16.88	0.9294	12.15	0.9481	11.60
	0 kg	0.9766	9.464	0.9349	16.67	0.9667	19.69	0.9078	15.78	0.9810	20.01	0.9218	14.62
Subject 3	1.5 kg	0.9634	13.77	0.9316	13.06	0.9417	12.66	0.9126	16.01	0.9622	11.28	0.9078	16.50
	3 kg	0.9345	16.67	0.9382	13.78	0.9470	13.05	0.9363	14.43	0.9672	13.27	0.9355	14.51
	0 kg	0.8847	18.46	0.8891	19.72	0.1142	78.67	0.1388	56.36	0.9254	15.57	0.9213	18.62
Subject 4	1.5 kg	0.9463	17.95	0.9147	18.23	0.7432	36.97	0.7774	38.19	0.8878	18.77	0.8045	23.43
	3 kg	0.9329	21.59	0.8744	18.40	0.8785	79.74	0.8508	29.37	0.9106	17.12	0.9074	20.04
	0 kg	0.9030	17.28	0.8381	25.19	0.9489	26.50	0.8732	17.82	0.9616	11.41	0.9031	19.40
Subject 5	1.5 kg	0.8336	18.24	0.7901	21.25	-0.6302	58.17	-0.6882	70.69	0.9246	15.89	0.9028	13.29
	3 kg	0.8989	20.56	0.8347	24.23	0.9499	97.20	0.9264	104.2	0.9772	15.77	0.9295	11.11
	0 kg	0.9408	15.91	0.9089	19.34	0.9504	41.71	0.9066	46.66	0.9528	15.21	0.9180	17.30
Subject 6	1.5 kg	0.9406	22.16	0.9468	15.91	0.8456	75.72	0.8487	87.73	0.8572	17.29	0.8812	18.10
	3 kg	0.8798	19.65	0.8863	18.88	0.8272	58.04	0.8220	54.78	0.8740	17.39	0.8725	17.10

of the system using a second batch of data, recorded in a different day.

The data acquired from the second experimental set were also used to calculate a new model, using the same model orders determined in the first experimental set. This way, it is possible to evaluate if the model orders calculated in one test set can be used to calculate a new model from a different data set.

To better determine the accuracy of the model, two performance parameters were used: correlation coefficient and the root-mean-square error (RMSE) between the estimated and the measured elbow joint angles. Table 2 shows the accuracy performance parameters for each participant and every test set. The different results for each method described above are presented in columns. The first data set was used to obtain a model that was used to estimate the joint angles that were compared to the measured angle values. Afterwards, the model obtained from the first experimental set was used with the sEMG inputs from the second experimental set to estimate the corresponding joint angles. Finally, using the same model orders chosen from the first data set, a new set of model parameters was obtained from the second data set, and the output was compared to the measured angle data.

6.4 Non-Linear System Model

The contents of this section have been partially published in (SOMMER; FORNER-CORDERO, 2018).

The non-linear system modeling was developed using the experiment in a smaller scale. As so, only data from two test subjects were considered.

Due to highly complex and nonlinear human dynamics, a good system identification method should be able to predict nonlinearities both on the input signals, since EMG signal presents nonlinearities, and output signals, because the movement of the elbow joint also presents nonlinearities in the form of gravitational forces, as an example. Considering these characteristics, the Hammerstein-Wiener model is a potential candidate for EMG-to-angle model estimation, since it is capable of estimating models from a black-box structure and predicting nonlinearities on both input and output signals.

6.4.1 Modeling

The chosen modeling technique to estimate the elbow joint angle using the sEMG data as input was the Hammerstein-Wiener model. The structure of the Hammerstein-Wiener model can be seen in fig. 24.

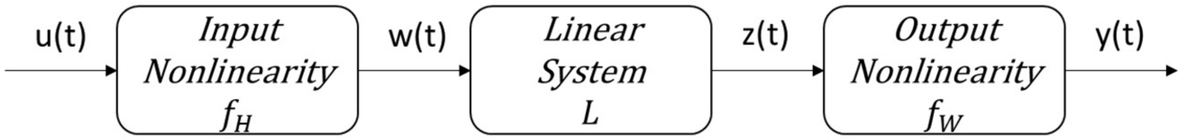

Figure 24: Hammerstein-Wiener model structure (Source: SOMMER; FORNER-CORDERO, 2018) .

The Hammerstein-Wiener model is a block-oriented model, consisting of a composition of a linear dynamic block and nonlinear memoryless blocks (WILLS et al., 2013). This model structure can be expressed as

$$y(t) = f_W(z(t)) \tag{6.9}$$

$$z(t) = L(w(t)) = \frac{B}{F}w(t) \tag{6.10}$$

$$w(t) = f_H(u(t)) \tag{6.11}$$

Here, $f_H(\cdot)$ is the input nonlinearity, $f_W(\cdot)$ is the output nonlinearity, $L(\cdot)$ is the Linear Time-Invariant system, $\frac{B}{F}$ is a transfer function, t is the time variable, $u(t)$ are the inputs, $y(t)$ is the output, $w(t)$ and $z(t)$ are internal variables.

f_H and f_W are memoryless nonlinearities, i.e. static functions where the output value at time t depends only on input value at time t.

Since the system being estimated is a MISO system the linear block is a transfer function vector in the form

$$\frac{B_i(q)}{F_i(q)} \tag{6.12}$$

Where $i = 1, 2, 3$ and q is the delay operator, representing the delay in time for each input to the system.

To determine the system, the orders of the numerator n_b and denominator n_f of the transfer function, as well as the input delays n_k, must be specified.

In order to find a solution a hard search was done using 1000 models with random orders ranging from 1 to 15. A window of 6s from the data vector was used to calibrate the model, while the entire data vector was used to validate the estimated model.

The following input and output nonlinearities were tested for each model: sigmoid network, wavelet network, piecewise linear function and one-dimensional polynomial.

Sigmoid network is a nonlinear estimator that combines a neural network with a sigmoid as the activation function (PATCHARAPRAKITI et al., 2011). It is represented by the equation 6.13:

$$y(u) = (u - r)PL + \sum_{i}^{n} a_i f((u - r)Qb_i - c_i) + d \tag{6.13}$$

where f is the sigmoid function, given by the following equation:

$$f(z) = \frac{1}{e^{-z} + 1} \tag{6.14}$$

when u is the input; y is the output; r is the regressor; Q is a nonlinear subspace; P a linear subspace; L is a linear coefficient; d is an output offset; b is a dilation coefficient; c a translation coefficient and a is an output coefficient. The sigmoid network is calculated in Matlab® (The Mathworks Inc, USA) through the use of an iterative search technique for estimating parameters.

Wavelet network is a feed-forward neural network using wavelet as an activation function, based on the following equation 6.15:

$$y(u) = (u - r)PL + \sum_{i}^{n} as_i f(bs(u - r)Q + cs) + \sum_{i}^{n} aw_i g(bw_i(u - r)Q + cw_i) + d \tag{6.15}$$

Where u is the input function; y is the output;Q is a nonlinear subspace; P is a linear subspace; L is a linear coefficient; d is output offset; as is a scaling coefficient; aw is a wavelet coefficient; bs is a scaling dilation coefficient; bw is a wavelet dilation coefficient; cs is a scaling translation coefficient and cw is a wavelet translation coefficient. The scaling function $f(.)$ is shown in equation 6.16 and wavelet function $g(.)$ in equation 6.17:

$$f(u) = exp(-0.5 * u' * u) \tag{6.16}$$

$$g(u) = (dim(u) - u' * u) * exp(-0.5 * u' * u) \tag{6.17}$$

Its parameters are determined in Matlab® (The Mathworks Inc, USA) by iterative minimization.

Piecewise linear nonlinearity is a piecewise-defined function, composed of straight-line sections (STANLEY, 2004). It is defined by the equation 6.18:

$$y = F(x, \theta) \tag{6.18}$$

Where y and x are scalars, and θ represents the parameters specifying the number of break points and the value of nonlinearity at the break points (MATHWORKS, 2016).

One-dimensional polynomial nonlinearity uses a one-dimensional polynomial as nonlinearity. The form of this nonlinearity can be expressed as in equation 6.19:

$$y = F(x)F(x) = c(1)x^n + c(2)x^{(n-1)} + ... + c(n)x + c(n+1) \tag{6.19}$$

Each model was compared to the reference angle using equations 6.6 and 6.7. The model orders that achieved the highest fitness value from these equations were chosen. The parameters of the models were estimated using time-domain data in Matlab® (The Mathworks Inc, USA).

The coefficient of determination R^2 was also used to measure the fitness of the proposed model.

$$R^2 = 1 - \frac{SS_{res}}{SS_{tot}} \tag{6.20}$$

Where

$$SS_{res} = \sum_{i=1}(y_i - \hat{y}_i)^2 \tag{6.21}$$

$$SS_{tot} = \sum_{i=1}(y_i - \bar{y})^2 \tag{6.22}$$

$$\bar{y} = \frac{1}{n}\sum_{i=1}^{n} y_i \tag{6.23}$$

Where $\bar{y}$ is the mean value of the measured angles.

6.4.2 Results

The model orders calculated are presented in table 3. Since the system is using three inputs, n_b, n_f and n_k are three dimensional. The input and output nonlinearity that achieved highest fitness values was the Wavelet Network.

Table 3: Model orders for each subject (Source: SOMMER; FORNER-CORDERO, 2018)
.

	n_b	n_f	n_k
Subject 1	4, 4, 0	9, 15, 0	12, 15, 0
Subject 2	7, 12, 15	2, 3, 14	11, 1, 11

Using the values from table 3 as the Hammerstein-Wiener model orders, we estimated the model for elbow joint angle using the sEMG data as input and compared the results to the experimentally measured values. As an example, figure 25 shows a comparison between the measured and estimated angle, for both continuous and intermittent movement, for subject 1.

Using the same model orders and parameters calculated previously, a second model estimation was performed using a second batch of data, recorded in a different day. An example of the result of this process is shown in figure 26, where the model calculated for subject 2 was used to estimate the elbow joint angle using the input data acquired from the second day of testing.

The data acquired from the second experimental set were also used to generate a new model, using the same model orders determined in first experimental set (table 3). This way, it is possible to evaluate if the same orders determined in one experiment can be carried over to tests performed in a different experimental set.

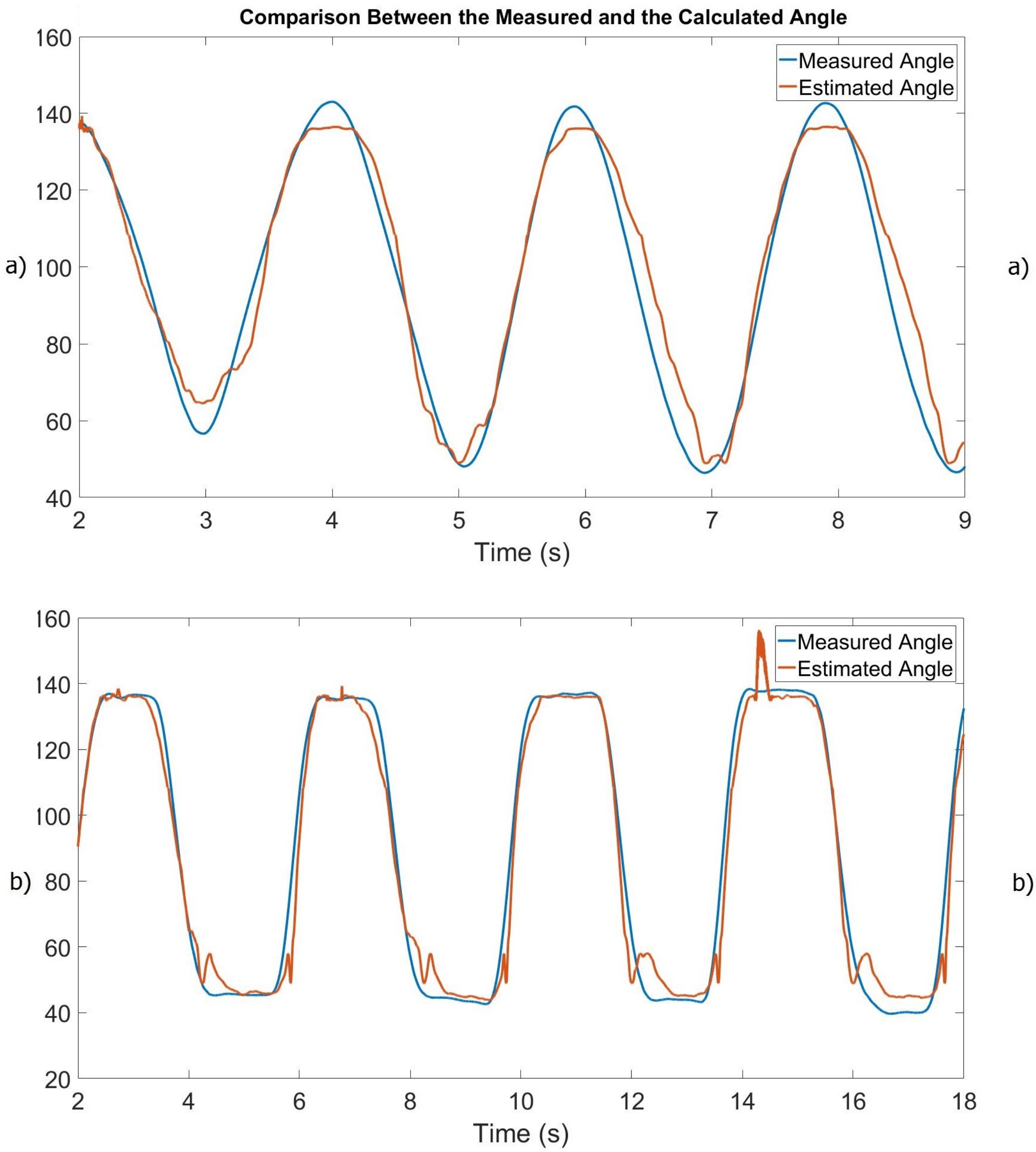

Figure 25: Comparison between the measured angle of the elbow joint and the angle calculated through the use of the estimated model, for subject 1, with a 1.5kg dumbbell. a) shows the comparison for the continuous movement and b) the comparison for the intermittent movement (Source: SOMMER; FORNER-CORDERO, 2018) .

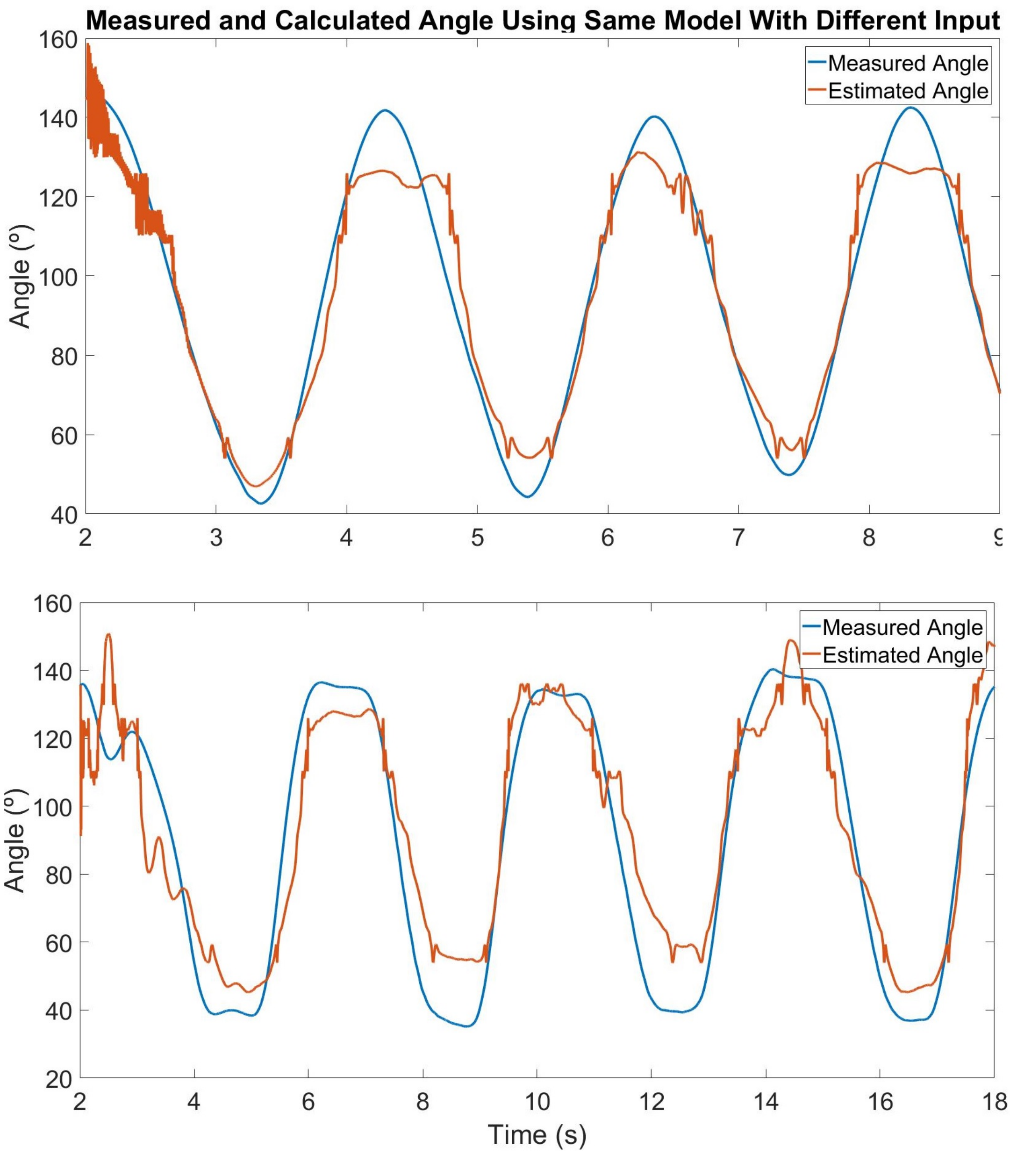

a)

b)

Figure 26: Comparison of the estimated and measured joint angle using the same model calculated with the first data set, but using the EMG data from the second test set as input for subject 2 with a 1.5kg dumbbell. a) shows the comparison for the continuous movement and b) the comparison for the discrete movement (Source: SOMMER; FORNER-CORDERO, 2018) .

To better determine the accuracy of the model, three performance parameters were used: the correlation coefficient, the determination coefficient and the root-mean-square Error (RMSE) between the estimated and the measured elbow joint angles. Table 4 shows the accuracy performance parameters for each participant and every test set. The different results for each method described above are presented in columns. First, using the first data set to estimate a model and comparing the result to the measured angle values; second, using the same model calculated for the first experimental set to estimate the angle, but using the data from the second experimental set as input to the model; and finally, using the same model orders chosen from the first experimental set, a new model was generated based on the second data set and comparing the output to the measured angle data.

Table 4: Correlation factor, coefficient of determination and root-mean-square error for the calculated and measured angle values (Source: SOMMER; FORNER-CORDERO, 2018) .

		Model Estimation, first test set						Same model, second test set						New model, same orders, second test set					
		Continuous			Intermittent			Continuous			Intermittent			Continuous			Intermittent		
		Correlation	R^2	RMSE	Correlation	R^2	RMSE	Correlation	R^2	RMSE	Correlation	R^2	RMSE	Correlation	R^2	RMSE	Correlation	R^2	RMSE
Subject 1	0 kg	0.9623	0.9232	9.394	0.9624	0.8932	12.91	0.8780	0.5114	17.86	0.9697	0.9205	9.647	0.9525	0.9044	7.898	0.9708	0.8602	12.79
	1.5 kg	0.9780	0.9480	7.390	0.9865	0.9714	6.846	0.9129	0.7403	14.21	0.9666	0.9339	8.870	0.9169	0.8400	11.15	0.9328	0.8470	13.50
	3 kg	0.9816	0.9499	6.796	0.9631	0.9200	11.477	0.9330	0.8526	10.31	0.7956	0.6161	22.70	0.9497	0.8912	8.860	0.9730	0.8923	12.03
Subject 2	0 kg	0.9729	0.9440	7.662	0.9620	0.9244	10.10	0.8825	0.7669	16.44	0.9330	0.8657	13.98	0.9787	0.9570	7.062	0.9620	0.9099	11.45
	1.5 kg	0.9596	0.9202	8.9476	0.9493	0.8859	11.62	0.9754	0.9425	7.927	0.9413	0.8683	14.09	0.9838	0.9673	5.976	0.9211	0.8482	15.12
	3 kg	0.9788	0.9556	6.733	0.9808	0.9612	6.540	0.8767	0.7668	15.35	0.9625	0.9191	11.02	0.9847	0.9688	5.614	0.9721	0.9431	9.246

The estimated models achieved correlation values of $94.90 \pm 3.92\%$, coefficient of determination of 0.8814 ± 0.0978 and RMSE values of $10.82 \pm 3.73°$

6.5 Discussion and Conclusions

This chapter proposed a method for determining the elbow joint angle based on the measurement of the sEMG of biceps brachii, triceps brachii and brachioradialis. The arm model was estimated using the data collected from the experiment and system identification methods. The system identification methods used were ARIMAX and Hammerstein-Wiener model with Wavelet Network as input and output nonlinearities. With the acquired sEMG data as input to the estimated model, it was possible to obtain an estimation of the elbow joint angle. Using the data from the IMU it was possible to validate the estimation based on sEMG.

The experimental data showed that it is possible to use the EMG data to estimate the joint angle, with prior knowledge of the weight being lifted, at least for the experimental conditions performed during the tests.

Both methods achieved good results in regards of the precision of angle estimation.

Since we are aiming at developing a real-time controller for the exoskeleton, a model with less complexity grants more advantageous characteristics, such as fewer calibration time and faster real-time calculation for angle estimation. For this reason, the linear model is the model chosen for further testing in real-time conditions.

In the next part, testing of the linear model, in a real-time condition, is performed.

PART IV

TESTING

7 CONTROL TESTING

To test the controller, the experiment must be conducted in two steps:

1. Similar to the tests performed for linear and nonlinear model calibration in chapter 6, a calibration procedure is made, recording the signal from the muscles, while the subject performs arm flexo-extension movements, with different weights. With this data, it is possible to estimate a dynamic model for the EMG-to-Angle relation;
2. With the dynamic model estimated, the input signal now serves as real-time input to the model, resulting in the corresponding angle estimation for the exoskeleton.

In the following sections, these experiments are described and the obtained results are shown.

7.1 Calibration

7.1.1 Equipment and Materials

7.1.1.1 EMG sensor

Even though the (FREEEMG 1000, BTS Bioengineering Corp., Italy) electrodes present high levels of accuracy, its larger dimensions and difficulty to establish communication with external hardware without dedicated software presents setbacks to its application in a real-time controller. For this reason, it is necessary to use another sensor for the acquisition of EMG data.

The chosen device for this end was the (Muscle Sensor V3, Sparkfun Electronics®, USA). Its low dimensions together with its ease of communication with microprocessors makes this device a great candidate for this specific application.

Connected to this sensor, a trio of electrodes must be connected: a pair of these electrodes is attached to the target muscle, while the third electrode must be attached to an electrically neutral portion of the body (such as a bony area), to serve as the ground reference for the device. The pair of electrodes placed at the muscle do the acquisition of EMG in an differential configuration, to filter noises in the EMG signal.

The device works by acquiring the signal from the electrodes; the signal is amplified by the AD8221 differential amplifier; the signal is amplified again in two steps with two TL084 operational amplifiers; then it is rectified by the 1N4148 diodes; the rectified signal is filtered in a low-pass filter; the signal is amplified by an adjustable gain amplifier. The Muscle Sensor V3 output can be connected directly to a microprocessor. An schematic of this device can be found at the Annex section of this work.

7.1.1.2 Microprocessor

The (FREEEMG 1000, BTS Bioengineering Corp., Italy) did the recording of the EMG data for the previous experiment. Since the (Muscle Sensor V3, Sparkfun Electronics®, USA) has been chosen for this new experiment, a microprocessor is required to do the recording of the data.

The chosen microprocessor for this end is the (Arduino UNO, Arduino, S.r.l., Italy). The Arduino Uno has low dimensions, making it portable; communication with the (Muscle Sensor V3, Sparkfun Electronics®, USA) is straightforward, requiring only the connection of the output from the EMG acquisition device to one of the analog inputs in the Arduino Uno; it has an embedded Analog-to-Digital converter; the ModExo exoskeleton already has an Arduino, being possible to modify the current software to record the data from the EMG acquisition device.

7.1.2 Subjects and experimental setup

One volunteer with no known neuromuscular deficit participated in the experiment. Surface Electromyography (sEMG) of one right arm muscle, biceps brachii, was recorded. sEMG was measured with 1 trio of electrodes connected to (Muscle Sensor V3, Sparkfun Electronics®, USA), that communicated with the Arduino, the latter recording the EMG data. Electrodes were placed with a separation of 20mm with the electrode diameter being 4mm. A pair of electrodes was placed on the biceps following the SENIAM guidelines (SENIAM, 2004). The third electrode was placed at the acromion. The sampling rate was of 20Hz. The user interface was the Arduino Serial Monitor.

7.1.3 Experimental protocol

The experimental protocol is similar to the experiment performed in chapter 6, being adapted to the new hardware setup. The subject sat on a chair, with the knees flexed at 90°, the back perpendicular to the ground. The back of the arm was leaning against a rubber support that was attached to the chair.

The subject was asked to perform consecutive elbow flexion and extension movements from 50° to 140° with a frequency of 0.5Hz. To achieve the desired movement speed a metronome was set at the speed of 60 BPM so that the subject could synchronize the movements with the sound of the metronome. This movement was repeated with 2kg and 3kg extra weight placed at the subject's hand.

All the data from the tests were transferred to Matlab® for further analysis and processing.

To reduce the complexity in processing the data and calibrating the model, the user did not perform intermittent flexion and extension movements.

7.1.4 Experimental data processing

The signal from the Muscle Sensor V3 is already rectified. A 10-point moving average was applied to further smooth the signal, to achieve a better result for the estimated model.

Since the position tracking data was sampled at 100 Hz while the EMG data was sampled at 20hz, all the position tracking data was resampled to 20 Hz.

7.1.5 Modeling

According to the results found in chapter 6, the FIR model is the linear model that achieves the best accuracy results. For this reason, it was the chosen model for application in the exoskeleton. In this case, the FIR model was estimated using data from the biceps muscle alone.

In order to find a solution, a hard search was done using 1000 different random model orders ranging from 1 to 10 for the n_a and n_b and 0 to 4 for n_k. Reduction of the n_k order has low impact in the model accuracy, while a reduction in its order reduces the computational effort of the microprocessor. The entire data window was used to calibrate the model, since the validation will be made through real time testing.

Each model was compared to the reference angle using equation 6.6. The orders of the model that achieved the highest fitness value were chosen. The parameters of the models were estimated using time-domain data in Matlab®.

7.2 Testing

7.2.1 Data processing

For the testing of the controller, the same hardware configuration was used. The EMG data was acquired by the (Muscle Sensor V3, Sparkfun Electronics®, USA), sending the data to the microprocessor. Data processing occurred as follows:

1. A 10-point moving average filter was applied to the EMG signal, replicating the same filter applied in the estimation of the model;
2. To simulate the detrending of the EMG data, the mean value of the EMG data used in the calibration procedure was subtracted in real time from the EMG signal;
3. Then, the data was used as input to the model calibrated on the previous section;
4. Since the output from the model is also a detrended value, to estimate the elbow joint angle the mean value of the elbow joint angle (acquired in the calibration procedure) was summed to the output of the model.

The model calculations were performed by the microprocessor.

The estimation of the joint angle can be represented as in 7.1.

$$A(q)\theta(n) = B(q)[V(n - n_k) - \bar{V}] + \bar{\theta} \tag{7.1}$$

Where $\theta(n)$ is the output angle of the elbow joint at discrete time n; $\bar{\theta}$ is the mean value of the elbow joint angle; $V(n)$ is the input, being the processed sEMG values from biceps brachii; $\bar{V}$ is the mean value of the sEMG signal; n_k is the delay for sEMG input; q is the delay operator; A and B are the model parameters, defined by:

$$A(q) = 1 + a_1 q^{-1} + \cdots + a_{n_a} q^{-n_a} \tag{7.2}$$

$$B(q) = 1 + b_1 q^{-1} + \cdots + b_{n_b} q^{-n_b+1} \tag{7.3}$$

Where n_a is the number of poles of the system; n_b is the number of zeros plus one.

To smooth the output signal, a low pass filter can be applied. It is interesting to use a low pass filter with a delay of no more than 100ms. The delay applied by a moving average filter can be calculated through the following equation

$$\frac{N-1}{2} * \frac{1}{f_{samp}} = delay \tag{7.4}$$

where N is the number of samples and f_{samp} is the sampling frequency. As a result, it is possible to apply a 5-point moving average filter to obtain a maximum delay of 100ms.

7.2.2 Results

The model orders calculated in 7.1.5 are presented in table 5.

Table 5: Model orders for test subject

n_a	n_b	n_k
0	10	4

Using the values presented in table 5 as the model orders, it was possible to test the model in real time, using the sEMG measurement from biceps brachii as input. The results of this estimation being the elbow joint angle. Figure 27 shows the comparison between the angle estimated from the model and the elbow joint angle measured from the test subject.

To determine the accuracy of the estimation, correlation coefficient, coefficient of determination and RMSE were used once more. Table 6 shows the accuracy performance parameters for the test sets.

Table 6: Correlation factor, coefficient of determination and Root-mean-square error for the real time estimated angle values

	Correlation	R^2	RMSE
0kg	0.8950	0.6958	18.16
2kg	0.9364	0.8004	14.61
3kg	0.9064	0.6792	18.55

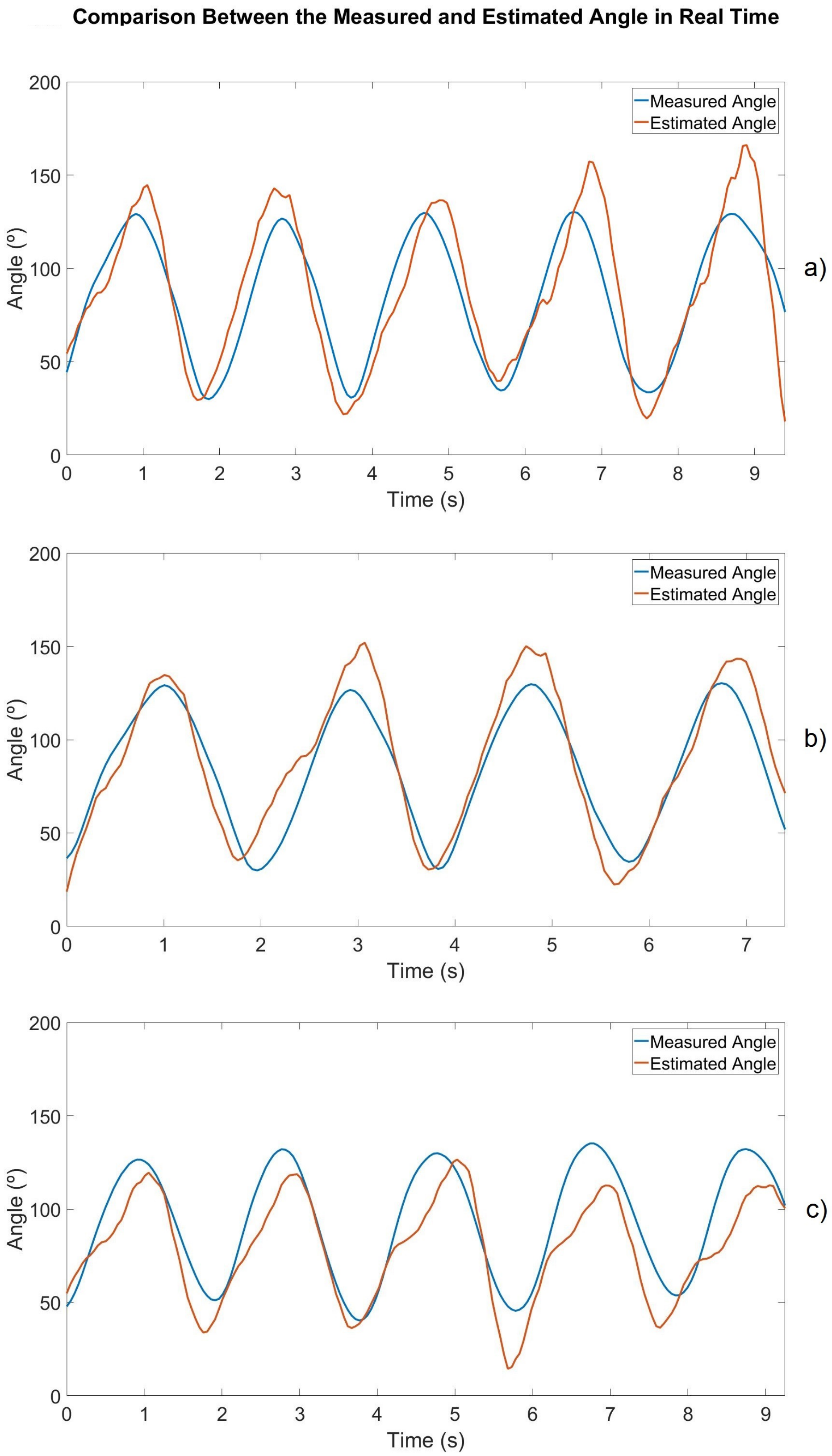

Figure 27: Comparison between the measured angle of the elbow joint and the angle calculated through the model in real time. a) shows the comparison for no extra weight b) the comparison for 2kg extra weight and c) the comparison for 3kg extra weight

7.3 Discussion and Conclusions

This chapter proposed a method and presented an experiment on the feasibility of real time exoskeleton control, using a linear model estimated through system identification. The system model was estimated using data collected from the experiment and a linear system identification method. With the model estimated, EMG data from biceps brachii was used as real time input for the model. As so, the output angle of the exoskeleton could be calculated.

The experimental data showed that the real time application of the EMG-driven controller was successful. Even though the results showed slightly inferior performance values to the offline testing, they are still deemed good compared to similar works already developed and referenced in this work.

The results of this testing have been accepted for publication in the conference IEEE EMBC 2019 (SUPLINO; SOMMER; FORNER-CORDERO, 2019).

PART V

DISCUSSIONS, CONCLUSIONS AND FUTURE WORK

8 DISCUSSIONS AND CONCLUSIONS

This work presented the design of an EMG-driven exoskeleton controller. Biomechatronics was combined with control design and system modeling to achieve the design of a controller that determines the intended movement and joint angle based on sEMG of the user's muscles.

Three different exoskeleton platforms, each with its own characteristics, were analyzed to determine which one better suited the application of the controller designed is this work. The exoskeleton platforms analyzed were the ETMICAE, ULEXO and ModExo. Built as an experimental workbench, the ModExo presents many advantages over the other exoskeletons, such as: embedded position and force sensors; easy-to-use communication between the platform, a computer and microprocessors; and robust and stable structure. For these reasons, the ModExo was the exoskeleton platform which better fitted the goals of this work. The main drawback of this option was the low computing capacities of its microprocessor.

Experimental procedures were conducted with six volunteers subjects to obtain EMG and angle data for the controller design. EMG from three arm muscles and elbow joint angle data were recorded in a controlled environment, where the test subjects were asked to perform continuous and intermittent elbow flexion and extensions, under three loading conditions: no load, 1.5kg and 3kg weights on the hand. The experiments were conducted in two different days for each subject. A total of 72 experimental sets were recorded. Data acquired through these experiments were used for system identification of the EMG-to-Angle relation.

Two different EMG-to-Angle model identification methods were proposed: one linear and the other nonlinear. For the linear method, four different modeling techniques were applied to determine which one best estimated the model. The modeling techniques were: ARX, ARMAX, ARIMAX and SS. The FIR model, a particular form of the ARX model, outperformed the other models and was the chosen modeling technique for linear system identification.

For the nonlinear method, the Hammerstein-Wiener model was chosen due to its capacity of estimating models from a black-box structure and predicting nonlinearities on both input and output signals.

Results for the linear model show similar precision values to those achieved by other authors (PANG et al., 2015; LIU; HERZOG; SAVELBERG, 1999; RAHMATIAN; MAHJOOB; HANACHI, 2016; MAMIKOGLU et al., 2016). For most of the simulations, the model achieved correlations above 90% and RMSE under 20°. Considering the worse results, the correlation was above 70% and the RMSE lower than 25°.

In most of the subjects, it was not possible to use the same model to estimate the elbow joint angle for tests conducted in different days. One way to address this problem would be to rescale the output signal to the angle range, minimizing the RMSE of the output signal. Since the EMG signals may change for one session to another, due to several reasons as slight change in electrode position, tissue properties or temperature (SODERBERG et al., 1975), it may not be possible to determine a model that estimates the joint angle for data acquired on different days or test setups, using the methods described in this work. Keeping this in mind, a solution would be to recalibrate the model at each session.

For subjects 2 and 3, using the same model for experimental data from two different days achieved correlation above 75% and RMSE below 32°. For subject 3, specifically, using the same model achieved values of correlation above 90% and RMSE below 20°. However, it is possible to note that the estimation is not as precise as it was when using the model identification data set as input, these results can be regarded as very good compared to other similar works. More investigation is required to determine if those models are capable of estimating the joint angle for any test conducted with these subjects.

The same model order calculated in the first test can be used for the subsequent test sessions, without a reduction in the accuracy of the predicted angle. This shows that, even considering that environmental noise affects the EMG signal, it does not change the system order. With the model orders already calculated, a recalibration procedure can be quickly applied, minimizing the problem of model non-repeatability.

For the nonlinear model, it achieved better results compared to the linear model. Even though other authors used the Hammerstein-Wiener model to determine EMG-to-Muscle Force relation instead of a EMG-to-Angle relation, the results show similar precision values (ABBASI-ASL et al., 2011; SEBASTIAN et al., 2010; CLANCY et al., 2012).

In most of the simulations, the model achieved values of correlation over 90%, coefficient of determination over 0.9 and RMSE under 15°. For both subjects, in the worst case, correlation was above 79%, coefficient of determination above 0.5 and RMSE below 23° when compared to the measured elbow joint angles.

As with the linear model, simulation results when using the same model for different data inputs are worse than the results presented when using the same data used for model calibration. But in this case, these results can be favorably compared to other similar works. Also, as before, the same model orders calculated through the first experimental set can be used for other test sessions, without loss of accuracy.

Linear system identification method was chosen and adapted for real time experiments. It was chosen over the nonlinear method since it could be better adapted to the available hardware and required less computational power. As such, the system identification method was adapted and implemented to function with a microprocessor and a different EMG acquisition equipment. A new experiment was conducted to calibrate a model using the new hardware.

With the linear model calibrated, testing of the controller in real time was performed. The test subject was asked to perform the same consecutive and continuous elbow flexion and extension performed in previous testing, with no extra weight, 2kg and 3kg extra weight. The results prove that the real time application of the EMG-driven exoskeleton control is possible in the proposed environment.

The real time controller achieved values of correlation, coefficient of determination and RMSE of $91.26\% \pm 2.14\%$, 0.7251 ± 0.0657 and $17.11° \pm 2.17°$, respectively. In the worst results, correlation was over 89%, coefficient of determination over 0.67 and RMSE under 20°. Care must be taken when inferring the applicability of this model to other test subjects. But as a proof of concept, the controller was successful in estimating the elbow joint angle in real time conditions.

In the end, the controller was capable of estimating the elbow joint angle using only EMG data as input, as long as the model was calibrated to the previously known load being carried by the user.

When referring to indirect results from this work, a database acquired from six test subjects, totaling 72 test sets of EMG and joint angle data, has been acquired. Even though this database has only been used for system identification modeling in this work, its data can be further used and analyzed under a multitude of different techniques, such as the Time Domain/Frequency Domain feature set, Neural Networks and mathematical morphological models (e.g. Hill's muscle model), to name a few.

9 FUTURE WORK

Much can be done to further improve the work presented in this dissertation. Some of the opportunities for improvement are described in the following section:

More extensive testing and acquisition of EMG and joint angle can be done, exploring more complex movements and replicating movements done on a daily basis. A longer acquisition time could also benefit models that require longer training periods, which is the case for some Neural Networks. For this end, a more portable hardware will be required, one that is capable of measuring EMG and angle data for long periods (days, even) with minimal negative impact on daily activities. This can further increase the accuracy of the model, as well as serving as data for models capable of performing more complex activities and movements.

Studying the possibility of estimating one single model for each subject, independent of the load applied to arm/exoskeleton, can result in an even better controller. One way to achieve this result would be to use a force sensor on the exoskeleton that measures the load applied. According to the readings of the sensor, a state machine could make a transition to the model corresponding to the applied load.

Hammerstein-Wiener models presented better results than the Linear system identification method. Application of the Hammerstein-Wiener model for real time testing could present better results than the ones obtained using the linear model. Exploration of different modeling techniques, such as Neural Networks, and the pairing with other extensively used morphological mathematical models, such as Hill's muscle models, can present even better models for the EMG-to-Angle relation.

More powerful hardware for real time testing could improve both the model accuracy as well as the output angle. Even though the Sparkfun Muscle Sensor V3 presented good results, the quality of signal acquisition is far from other equipment, like the BTS (FREEEMG 1000, BTS Bioengineering Corp., Italy). An EMG acquisition device that is both portable and accurate would be the ideal hardware for this application. Also, a wireless communication between the electrodes and the processing unit would also present more freedom of movement for the user.

A subject-independent model, that can estimate joint angles for a large group of subjects, would present a huge improvement by being able to skip the model calibration procedure necessary between each test session.

ModExo was well suited as a platform for testing and studying the proposed methods. But it has little to no application for movement assistance in real life activities. The ideal scenario would be to apply the controller proposed in this work in an exoskeleton designed for movement assistance in daily activities. When the work on the construction of ETMICAE is finished, it can prove to be a great platform for further testing of the proposed controller.

Above all, this work is a product of collaborative effort between many people, from colleagues and professors at Escola Politécnica - USP to many theorists and specialists in engineering and medicine. And it is through this collaborative effort that this work will achieve even higher standards. As many have contributed to this work, I hope this work will serve as contribution for many others to come.

REFERENCES

ABBASI-ASL, R. et al. Estimation of muscle force with emg signals using hammerstein-wiener model. In: OSMAN, N. A. A. et al. (Ed.). *5th Kuala Lumpur International Conference on Biomedical Engineering 2011*. Berlin, Heidelberg: Springer Berlin Heidelberg, 2011. p. 157–160. ISBN 978-3-642-21729-6.

AL-TIMEMY, A. H. et al. A preliminary investigation of the effect of force variation for myoelectric control of hand prosthesis. In: *2013 35th Annual International Conference of the IEEE Engineering in Medicine and Biology Society (EMBC)*. [S.l.: s.n.], 2013. p. 5758–5761. ISSN 1094-687X.

ALTER, R. *Bioelectric control of prostheses*. [S.l.], 1966.

AMUNDSON, K. et al. Development of hybrid hydraulic-electric power units for field and service robots. *Advanced Robotics*, v. 20, p. 1015–1034, 2006.

ANAM, K.; AL-JUMAILY, A. A. Active exoskeleton control systems: State of the art. *Procedia Engineering*, v. 41, p. 988 – 994, 2012. ISSN 1877-7058.

AUNG, Y.; AL-JUMAILY, A. Estimation of upper limb joint angle using surface emg signal. *International Journal of Advanced Robotic Systems*, v. 10, 2013.

AZAB, A. M.; ARVANCH, M.; MIHAYLOVA, L. S. Estimation of joint angle based on surface electromyogram signals recorded at different load levels. In: *2017 39th Annual International Conference of the IEEE Engineering in Medicine and Biology Society (EMBC)*. [S.l.: s.n.], 2017. p. 2538–2541. ISSN 1557-170X.

BATTYE, C. K.; NIGHTINGALE, A.; WHILLIS, J. The use of myo-electric currents in the operation of prostheses. *Bone & Joint Journal*, Bone and Joint Journal, v. 37-B, n. 3, p. 506–510, 1955. ISSN 0301-620X.

BOTTOMLEY, A. H. Myo-electric control of powered prostheses. *Bone & Joint Journal*, Bone and Joint Journal, v. 47-B, n. 3, p. 411–415, 1965. ISSN 0301-620X.

CHEN, X.; CHEN, S.; DAN, G. Control of powered prosthetic hand using multidimensional ultrasound signals: A pilot study. In: STEPHANIDIS, C. (Ed.). *Universal Access in Human-Computer Interaction. Applications and Services: 6th International Conference, UAHCI 2011, Held as Part of HCI International 2011, Orlando, FL, USA, July 9-14, 2011, Proceedings, Part IV*. Berlin, Heidelberg: Springer Berlin Heidelberg, 2011. p. 322–327. ISBN 978-3-642-21657-2.

CHILDRESS, D. S.; HOLMES, D. W.; BILLOCK, J. N. Ideas on myoelectric prosthetic systems for upper-extremity amputees. *The Control of Upper-extremity Prostheses and Orthoses*, Charles C. Thomas, p. 86–106, 1971.

CHU, A.; KAZEROONI, H.; ZOSS, A. On the biomimetic design of the berkeley lower extremity exoskeleton (bleex). In: *Proceedings of the 2005 IEEE International Conference on Robotics and Automation*. [S.l.: s.n.], 2005. p. 4345–4352. ISSN 1050-4729.

CLANCY, E. A. et al. Identification of constant-posture emg-torque relationship about the elbow using nonlinear dynamic models. *IEEE Transactions on Biomedical Engineering*, v. 59, n. 1, p. 205–212, Jan 2012. ISSN 0018-9294.

CYBERDYNE. *Cyberdine Products, Available in : https://www.cyberdyne.jp/english/. Access in 16/06/2017*. 2007.

DOLLAR, A. M.; HERR, H. Lower extremity exoskeletons and active orthoses: Challenges and state-of-the-art. *IEEE Transactions on Robotics*, v. 24, n. 1, p. 144–158, Feb 2008. ISSN 1552-3098.

ENGLEHART, K.; HUDGINS, B. A robust, real-time control scheme for multifunction myoelectric control. *IEEE Transactions on Biomedical Engineering*, v. 50, n. 7, p. 848–854, July 2003. ISSN 0018-9294.

ENGLEHART, K. et al. Classification of the myoelectric signal using time-frequency based representations. *Medical Engineering & Physics*, v. 21, n. 6–7, p. 431 – 438, 1999. ISSN 1350-4533.

ESQUENAZI, A. New bipedal locomotion option for individuals with thoracic level motor complete spinal cord injury. *J. Spinal Res. Found.*, v. 8, p. 26–28, 2013.

EVANS, H. B. et al. Signal processing for proportional myoelectric control. *IEEE Transactions on Biomedical Engineering*, BME-31, n. 2, p. 207–211, Feb 1984. ISSN 0018-9294.

FARINA, D.; MERLETTI, R.; ENOKA, R. M. The extraction of neural strategies from the surface emg: an update. *Journal of Applied Physiology*, American Physiological Society, v. 117, n. 11, p. 1215–1230, 2014. ISSN 8750-7587.

FINEBERG, D. B. et al. Vertical ground reaction force-based analysis of powered exoskeleton-assisted walking in persons with motor-complete paraplegia. *The Journal of Spinal Cord Medicine*, v. 36(4), p. 313–321, 2013.

FOUGNER, A. et al. Cancellation of force induced artifacts in surface emg using fsr measurements. *Proc. Myoelectric Controls Symp. (MEC)*, 2008.

FOUGNER, A. et al. Resolving the limb position effect in myoelectric pattern recognition. *IEEE Transactions on Neural Systems and Rehabilitation Engineering*, v. 19, n. 6, p. 644–651, Dec 2011. ISSN 1534-4320.

FRANCESCHINI, M. et al. Reciprocating gait orthoses: A multicenter study of their use by spinal cord injured patients. *Archives of Physical Medicine and Rehabilitation*, v. 78, n. 6, p. 582 – 586, 1997. ISSN 0003-9993.

GARCIA, E.; SATER, J. M.; MAIN, J. Exoskeletons for human performance augmentation (ehpa) : A program summary. *Journal of the Robotics Society of Japan*, v. 20, n. 8, p. 822–826, 2002.

GHAN, J.; KAZEROONI, H. System identification for the berkeley lower extremity exoskeleton (bleex). In: *Proceedings 2006 IEEE International Conference on Robotics and Automation, 2006. ICRA 2006.* [S.l.: s.n.], 2006. p. 3477–3484. ISSN 1050-4729.

HAYASHIBE, M.; GUIRAUD, D.; POIGNET, P. EMG-to-force estimation with full-scale physiology based muscle model. In: *IROS'09: International Conference on Intelligent Robots and Systems*. St. Louis, MO, United States: IEEE/RSJ, 2009. p. 1621–1626.

HOGAN, N.; MANN, R. W. Myoelectric signal processing: Optimal estimation applied to electromyography - part i: Derivation of the optimal myoprocessor. *IEEE Transactions on Biomedical Engineering*, BME-27, n. 7, p. 382–395, July 1980. ISSN 0018-9294.

HOGAN, N.; MANN, R. W. Myoelectric signal processing: Optimal estimation applied to electromyography - part ii: Experimental demonstration of optimal myoprocessor performance. *IEEE Transactions on Biomedical Engineering*, BME-27, n. 7, p. 396–410, July 1980. ISSN 0018-9294.

HUDGINS, B.; PARKER, P.; SCOTT, R. N. A new strategy for multifunction myoelectric control. *IEEE Transactions on Biomedical Engineering*, v. 40, n. 1, p. 82–94, Jan 1993. ISSN 0018-9294.

IBGE. Censo demográfico 2010 - características gerais da população, religião e pessoas com deficiência. IBGE, Rio de Janeiro, Brazil, 2012.

ISIDORI, A.; NICOLO, F. A device for the detection and measurement of some parameters of myoelectric potentials. *Report no. 11, Electrotechnical Institute, University of Rome*, Electrotechnical Institute, University of Rome, 1966.

JIANG, N.; ENGLEHART, K. B.; PARKER, P. A. Extracting simultaneous and proportional neural control information for multiple-dof prostheses from the surface electromyographic signal. *IEEE Transactions on Biomedical Engineering*, v. 56, n. 4, p. 1070–1080, April 2009. ISSN 0018-9294.

KATO, A. et al. Estimating a joint angle by means of muscle bulge movement along longitudinal direction of the forearm. In: *2015 IEEE International Conference on Robotics and Biomimetics (ROBIO)*. [S.l.: s.n.], 2015. p. 614–619.

KAWAMOTO, H. et al. Voluntary motion support control of robot suit hal triggered by bioelectrical signal for hemiplegia. In: *2010 Annual International Conference of the IEEE Engineering in Medicine and Biology*. [S.l.: s.n.], 2010. p. 462–466. ISSN 1094-687X.

KAZEROONI, H. The berkeley lower extremity exoskeleton. In: ______. *Field and Service Robotics: Results of the 5th International Conference*. Berlin, Heidelberg: Springer Berlin Heidelberg, 2006. p. 9–15. ISBN 978-3-540-33453-8.

KENNEY, L. et al. Dimensional change in muscle as a control signal for powered upper limb prostheses: a pilot study. *Medical Engineering & Physics*, v. 21, n. 8, p. 589–597, 1999. ISSN 1350-4533.

LENZI, T. et al. Intention-based emg control for powered exoskeletons. *IEEE Transactions on Biomedical Engineering*, v. 59, n. 8, p. 2180–2190, Aug 2012. ISSN 0018-9294.

LIU, M.; HERZOG, W.; SAVELBERG, H. Dynamic muscle force predictions from emg: An artificial neural network approach. *Journal of Electromyography and Kinesiology*, v. 9, n. 6, p. 391–400, 1999.

LOSIER, Y.; ENGLEHART, K.; HUDGINS, B. A control system for a powered prosthesis using positional and myoelectric inputs from the shoulder complex. In: *2007 29th Annual International Conference of the IEEE Engineering in Medicine and Biology Society*. [S.l.: s.n.], 2007. p. 6137–6140. ISSN 1094-687X.

MACKAY, J. et al. *The Atlas of Heart Disease and Stroke*. [S.l.]: World Health Organization, 2004. (Academic Search Complete). ISBN 9789241562768.

MAMIKOGLU, U. et al. Elbow joint angle estimation by using integrated surface electromyography. In: . [S.l.: s.n.], 2016. p. 785–790.

MATHWORKS. *armax. Available in: https://www.mathworks.com/help/ident/ref/armax.html. Access in 06/07/2019.* 2015.

MATHWORKS. *pwlinear. Available in: https://www.mathworks.com/help/ident/ref/pwlinear.html. Access in 06/07/2019.* 2016.

MERRIAMWEBSTERDICTIONARY. *Biomimetics definition. Available in: https://www.merriam-webster.com/dictionary/biomimetics. Access in 11/07/2017.* 2009.

MIRANDA, A. B. W.; FORNER-CORDERO, A. Upper limb exoskeleton control based on sliding mode control and feedback linearization. In: *2013 ISSNIP Biosignals and Biorobotics Conference: Biosignals and Robotics for Better and Safer Living (BRC)*. [S.l.: s.n.], 2013. p. 1–6. ISSN 2326-7844.

NIELSEN, J. L. G. et al. Enhanced emg signal processing for simultaneous and proportional myoelectric control. In: *2009 Annual International Conference of the IEEE Engineering in Medicine and Biology Society*. [S.l.: s.n.], 2009. p. 4335–4338. ISSN 1094-687X.

NIGHTINGALE, J. Microprocessor control of an artificial arm. *Journal of Microcomputer Applications*, v. 8, n. 2, p. 167 – 173, 1985. ISSN 0745-7138.

OTSUKA, T. et al. Development of upper-limb type hal and reaching movement for meal-assistance. In: *2011 IEEE International Conference on Robotics and Biomimetics*. [S.l.: s.n.], 2011. p. 883–888.

PANG, M. et al. Electromyography-based quantitative representation method for upper-limb elbow joint angle in sagittal plane. *Journal of Medical and Biological Engineering*, v. 35, n. 2, p. 165–177, 2015.

PARKER, P.; STULLER, J.; SCOTT, R. Signal processing for the multistate myoelectric channel. *Proceedings of the IEEE*, v. 65, n. 5, p. 662–674, 1977.

PATCHARAPRAKITI, N. et al. Modeling of photovoltaic grid connected inverters based on nonlinear system identification for power quality analysis. 2011.

PHILIPSON, L. Adaptable myoelectric prosthetic control with functional visual feedback using microprocessor techniques. *Medical and Biological Engineering and Computing*, v. 23, n. 1, p. 8–14, 1985. ISSN 1741-0444.

PONS, J. *Wearable Robots: Biomechatronic Exoskeletons*. [S.l.]: Wiley, 2008. ISBN 9780470987650.

RAHMATIAN, S.; MAHJOOB, M.; HANACHI, M. Continuous estimation of ankle joint angular position based on the myoelectric signals. In: . [S.l.: s.n.], 2016. p. 158–163.

ROSE, W. *Electromyogram Analysis. Available in: https://www1.udel.edu/biology/rosewc/kaap686/notes/EMG%20analysis.pdf. Access in 12/11/2016*. 2011.

SANKAI, Y. Hal: Hybrid assistive limb based on cybernics. In: _____. *Robotics Research: The 13th International Symposium ISRR*. Berlin, Heidelberg: Springer Berlin Heidelberg, 2011. p. 25–34. ISBN 978-3-642-14743-2.

SEBASTIAN, A. et al. Analysis of emg-force relation using system identification and hammerstein-wiener models. *ASME 2010 Dynamic Systems and Control Conference*, v. 1, p. 381–388, Jan 2010. ISSN 0018-9294.

SENIAM. *Recommendations for sensor locations in arm or hand muscles., Available in : http://seniam.org/. Access in 10/11/2016*. 2004.

SILVA, J.; CHAU, T.; GOLDENBERG, A. Mmg-based multisensor data fusion for prosthesis control. In: *Proceedings of the 25th Annual International Conference of the IEEE Engineering in Medicine and Biology Society (IEEE Cat. No.03CH37439)*. [S.l.: s.n.], 2003. v. 3, p. 2909–2912 Vol.3. ISSN 1094-687X.

SLOTINE, J.-J. E.; LI, W. *Applied nonlinear control*. Upper Saddle River, NJ: Pearson, 1991.

SODERBERG, G. et al. *Selected Topics in Surface Electromyography for Use in the Occupational Setting: Expert Perspectives*. [S.l.]: U.S. Dept. of Health and Human Services, Public Health Service, CDC, National Institute for Occupational Safety and Health, 1975. (DHHS publication).

SOMMER, L. F. Upper limb exoskeleton with one degree of freedom. *Undergraduate Thesis*, Dept. Mechatronic Eng. and Mech. Systems, Escola Politécnica, University of São Paulo, 2015.

SOMMER, L. F. et al. Elbow joint angle estimation with surface electromyography using autoregressive models. In: *2018 40th Annual International Conference of the IEEE Engineering in Medicine and Biology Society (EMBC)*. [S.l.: s.n.], 2018. p. 1472–1475. ISSN 1558-4615.

SOMMER, L. F.; FORNER-CORDERO, A. Elbow joint angle estimation from surface electromyography using hammerstein-wiener models. In: *2018 7th IEEE International Conference on Biomedical Robotics and Biomechatronics (Biorob)*. [S.l.: s.n.], 2018. p. 1044–1049. ISSN 2155-1782.

SOUIT, C. Design and prototyping of a development platform for exoskeleton research. *Master's Dissertation*, Dept. Mechatronic Eng. and Mech. Systems, Escola Politécnica, University of São Paulo, 2016.

SOUZA, R. S. Design and prototyping of a development platform for exoskeleton research. *Master's Dissertation*, Dept. Mechatronic Eng. and Mech. Systems, Escola Politécnica, University of São Paulo, 2018.

STANLEY, W. D. *Technical Analysis And Applications With Matlab*. [S.l.]: Cengage Learning, 2004. 143 p. ISBN 9781401864811.

STAVDAHL, O.; GRONNINGSAETER, A.; E.MALVIG, K. Ultrasound based estimation of muscle contraction. *Dept, of Engineering Cybernetics, Norwegian University of Science and Technology,*, 1997.

STAVDAHL, O. et al. Multimodal input device with smeg and contact force sensors. *Proc. Myoelectric Controls Symp. (MEC)*, 2011.

STEGER, R.; KIM, S. H.; KAZEROONI, H. Control scheme and networked control architecture for the berkeley lower extremity exoskeleton (bleex). In: *Proceedings 2006 IEEE International Conference on Robotics and Automation, 2006. ICRA 2006.* [S.l.: s.n.], 2006. p. 3469–3476. ISSN 1050-4729.

SUPLINO, L. O.; SOMMER, L. F.; FORNER-CORDERO, A. Emg-based control in a test platform for exoskeleton with one degree of freedom. 2019.

TALATY, M.; ESQUENAZI, A.; BRICENO, J. E. Differentiating ability in users of the rewalk^{TM} powered exoskeleton: An analysis of walking kinematics. In: *2013 IEEE 13th International Conference on Rehabilitation Robotics (ICORR)*. [S.l.: s.n.], 2013. p. 1–5. ISSN 1945-7898.

TSUKAHARA, A. et al. Restoration of gait for spinal cord injury patients using hal with intention estimator for preferable swing speed. *IEEE Transactions on Neural Systems and Rehabilitation Engineering*, v. 23, n. 2, p. 308–318, March 2015. ISSN 1534-4320.

VALIENTE, A. Design of a quasi-passive parallel leg exoskeleton to augment load carrying for walking. *Master's Thesis*, Dept. Mech. Eng., Massachusetts Inst. Technol., Cambridge, August, 2005.

VONSCHRADER, S.; LEE, G. Disability statistics from the current population survey (cps). Cornell University Yang Tan Institute (YTI), 2017.

WALSH, C. J. Biomimetic design of an under-actuated leg exoskeleton for load-carrying augmentation. *Master's Thesis*, Dept. Mech. Eng., Massachusetts Inst. Technol., Cambridge, February, 2006.

WALSH, C. J.; ENDO, K.; HERR, H. A quasi-passive leg exoskeleton for load-carrying augmentation. *International Journal of Humanoid Robotics*, v. 4, n. 3, p. 487–506, 2007.

WATKINS, K. Human development report 2005. American Physiological Society, 2005.

WILLS, A. et al. Identification of hammerstein–wiener models. *Automatica*, v. 49, n. 1, p. 70 – 81, 2013. ISSN 0005-1098.

YOUNG, A. J.; FERRIS, D. P. State of the art and future directions for lower limb robotic exoskeletons. *IEEE Transactions on Neural Systems and Rehabilitation Engineering*, v. 25, n. 2, p. 171–182, Feb 2017. ISSN 1534-4320.

ZEILIG, G. et al. Safety and tolerance of the rewalk exoskeleton suit for ambulation by people with complete spinal cord injury: a pilot study. *J Spinal Cord Med.*, v. 35(2), p. 96–101, 2012.

ZOSS, A.; KAZEROONI, H. Design of an electrically actuated lower extremity exoskeleton. *Advanced Robotics*, v. 20, n. 9, p. 967–988, 2006.

ZOSS, A. B.; KAZEROONI, H.; CHU, A. Biomechanical design of the berkeley lower extremity exoskeleton (bleex). *IEEE/ASME Transactions on Mechatronics*, v. 11, n. 2, p. 128–138, April 2006. ISSN 1083-4435.

APPENDIX A – ETMICAE CALCULATIONS, SIMULATIONS AND MATERIALS

A.1 Hip

A.1.1 Applied Forces

The weight of the user will be applied at the back support, attached to the hip base. For design purposes, the maximum user weight will be 1000 N. When walking with the exoskeleton, there is the possibility of the user tilting forward his upper body. The torque applied to the hip base due to this misalignment between the upper body and the base is considered as a 25 Nm torque. The torque applied at the joints is equal to 250 Nm that is the maximum torque applied by the motors to the joints.

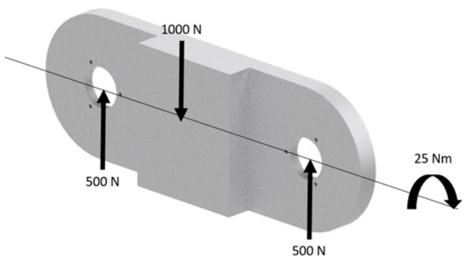

Figure 28: Acting forces on the base

A.1.2 Materials

Aluminum was chosen for the structural plates as well as for the joints due to its low weight and high resistance/weight coefficient.

The shafts will be constituted of steel, since they will support high loads. Because of its low dimensions, it is not critical the usage of low weight materials.

For the coupling of the shafts, ball bearings will be used so that the joints can rotate with low friction coefficient, as well as being capable of enduring the high loads applied. The chosen ball bearings were DIN 652 SKF with 2 RS1.

To avoid interference between the two parts of the joints, a Permaglide® thrust washer model PAW 26 will be used. This thrust washer has the necessary resistance to withstand the applied loads. Also, it is low weight and easier to assemble compared to axial bearings.

The cover attached to the shaft will be made of aluminum.

A.1.3 Calculations and simulations

Permaglide® PAW 26 Thrust Washer:

Torque at the hip due to the misalignment between the upper body and the rotation axis of the hip is considered as a 25 Nm torque. This torque will be supported by the thrust washer. That way:

$$M = 2 \cdot F \cdot \frac{\frac{D_e}{2} + \frac{D_i}{2}}{2} \tag{A.1}$$

$$A = \frac{\frac{\pi}{4}(D_e^2 - D_i^2)}{2} \tag{A.2}$$

$$\sigma = \frac{F}{A} \tag{A.3}$$

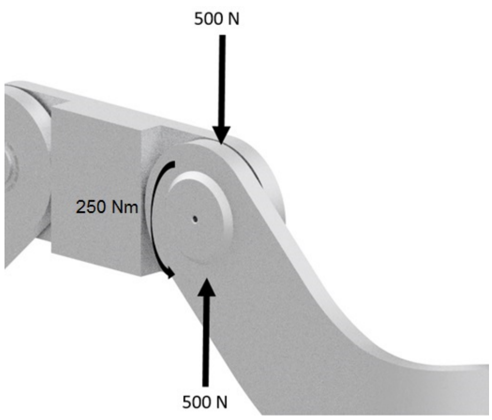

Figure 29: Acting forces on the abduction/adduction joint

Figure 30: Acting forces on the flexion/extension joint

Where M is the torque applied to the hip, F is the reaction force in the thrust washer and cover of the joint, D_e and D_i are the external and internal diameter of the thrust washer, respectively, A is the thrust washer area that will support the load and σ is the load.

Resulting in:

$$\sigma \cong 1.5MPa < \sigma_{crit}$$

Therefore, the PAW 26 thrust washer is suitable to be used.

DIN 625 SKF with 2 RS1 (SKF 61902-2RS1) ball bearing:

Chosen through the SKF™ bearing selection tool, for a load equal to 500 N and lifespan of 10000 hours. The tool can be found at: http://www.skf.com/group/knowledge-centre/engineering-tools/skfbearingselect.html

All components were numerically simulated at the Autodesk™ Inventor 2017 software.

A.2 Knee

A.2.1 Applied forces

The forces applied at the knee joint are the torque that the motor applies at the joint and the weight of the user and exoskeleton.

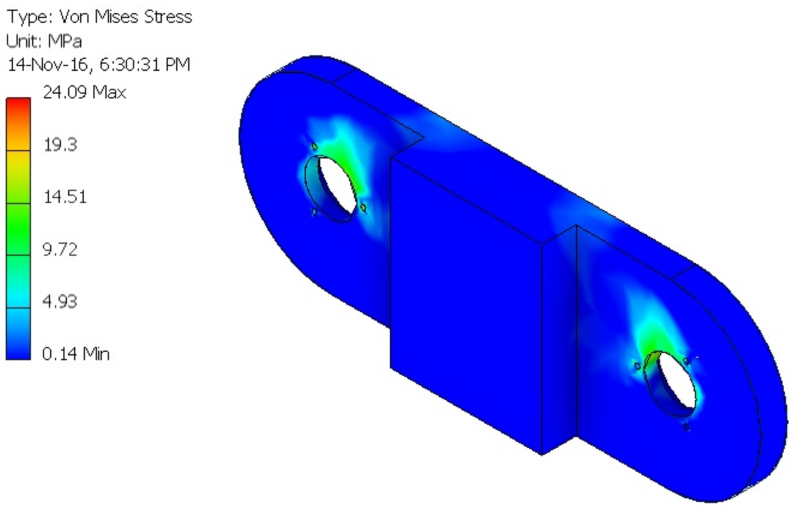

Figure 31: Numerical simulation of the base

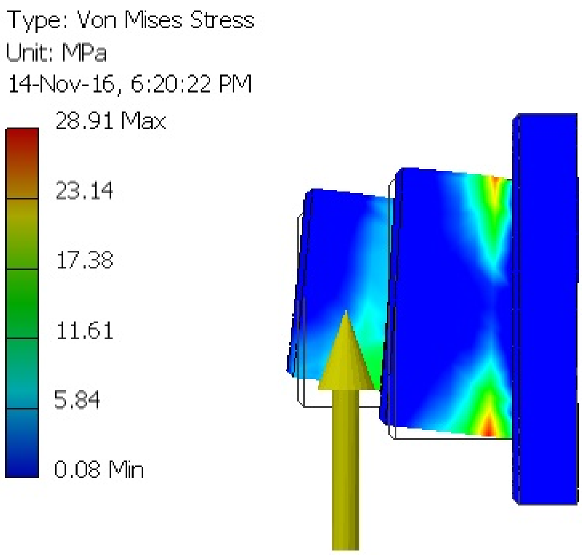

Figure 32: Numerical simulation of the joint shafts

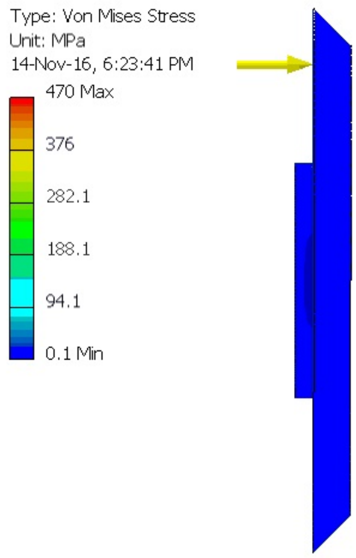

Figure 33: Numerical simulation of the cover

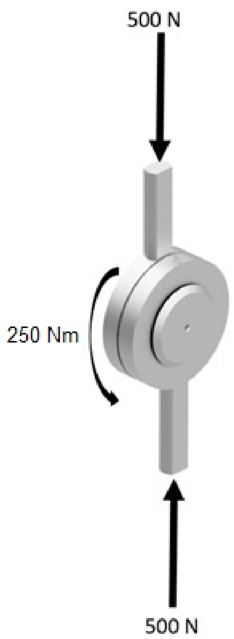

Figure 34: Forces applied to the knee joint

A.2.2 Materials

Aluminum is the metal constituting the joints. This material was chosen for its low weight and high resistance/weight coefficient.

For the bars, steel bars will be used for its high resistance and easy acquisition.

For the same reasons stated at the hip, the shafts will be made of steel.

Like before, DIN 625 SKF with 2 RS1 ball bearings and PAW 26 Permaglide® thrust washers will be used.

A.2.3 Calculations and simulations

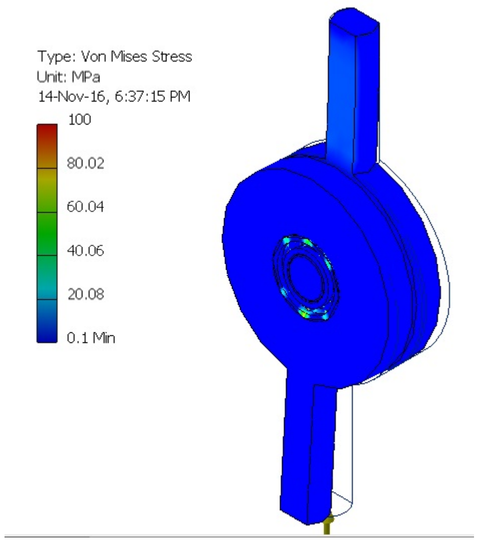

Figure 35: Numerical simulation of the knee joint

APPENDIX B – ACTUATOR CONTROL

Human limb and exoskeleton mechanics are complex and nonlinear. To account for this complexity, it is necessary to model the interaction between exoskeleton and the human limb when exposed to an external load.

In this annex, a study of two control methods for the actuation of the exoskeleton is conducted: impedance control and sliding mode control.

B.1 Exoskeleton Model

B.1.1 Exoskeleton

In order to present this controller, we will use the upper limb exoskeleton described in chapter 4. It has one degree of freedom on the elbow joint, actuated by a 12V DC motor (578VA, Mabuchi Motor Co., ltd., Japan) with a Power Window Lifter gear transmission. The transmission has a 10:1 reduction ratio. The structure of the exoskeleton is constructed on aluminum.

The exoskeleton is illustrated in figure 36. When the user tries to flex his arm, an electrical voltage is acquired by electrodes placed on the skin on the biceps brachii. The (Muscle Sensor V3, Sparkfun Electronics®, USA), was used to measure the EMG. It does the biceps muscle voltage recording, rectification, low-pass filtering and amplification. This signal is sent to a microprocessor (ATmega328P, Microchip Technology Inc., USA), that makes the analog-to-digital conversion and applies a moving average filter. Finally the voltage signal is transformed into a desired joint angle. Equation B.1 shows the equation that gives the desired joint angle as a function of the EMG sensor voltage. A linear relationship between the angular position and the measured voltage was chosen. The equation was defined by measuring the EMG signal when the arm was fully extended and when the arm was on a flexed position and linearly scaling it to the minimum angle of 0 and maximum angle of $\frac{\pi}{2}$. It is important to note that the voltage from the EMG sensor is never zero. Even at a relaxed position, the sensor measures a residual voltage level of -0.29V.

$$\theta_d = -0.29 + 0.582 * V_{emg} \tag{B.1}$$

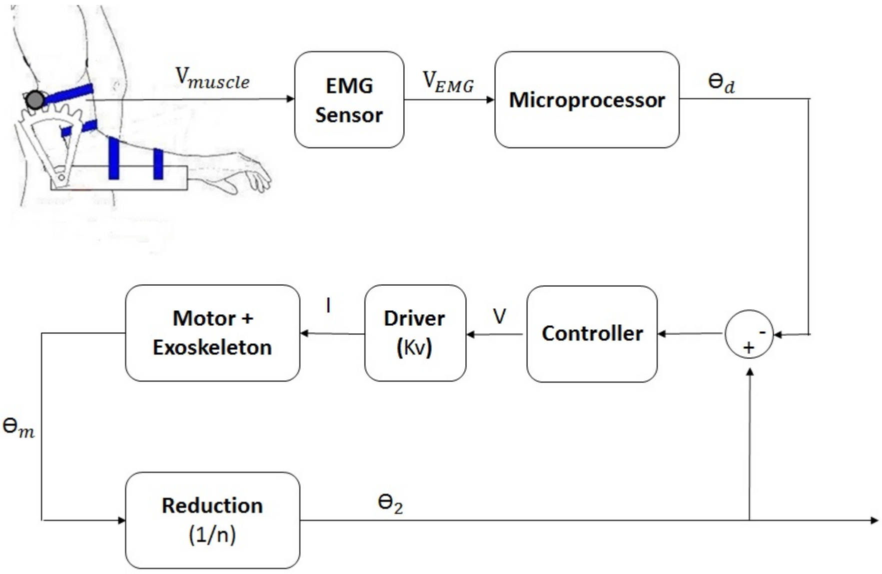

Figure 36: Diagram showing the exoskeleton block diagram control

With the desired joint angle the pulse-width modulation (PWM) magnitude sent to the motor driver is calculated with a control logic in order to control the motor that actuates the exoskeleton. This control logic will be further studied in the next section. The motor driver input is the PWM voltage (V) and its output is an electrical current (I). Equation B.2 shows the relationship between PWM voltage and motor current:

$$I = K_v * V \tag{B.2}$$

where $K_v = 1.42$ is the driver gain, V is the voltage applied to the driver and I is the output current of the driver.

The output electrical current from the driver goes to the motor, actuating in the exoskeleton and consequently moving the user's forearm.

B.1.2 Modeling

Even though the exoskeleton has only one degree of freedom on the elbow joint, the shoulder angle should also be considered because it influences the forces applied to the exoskeleton and the arm. The exoskeleton can be modeled as two segments: the upper arm (between shoulder and elbow) and the forearm (between elbow and wrist).

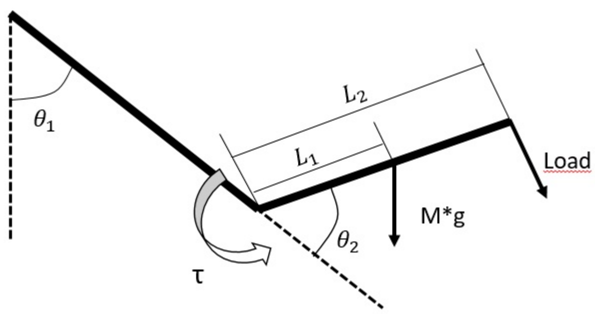

Figure 37: Free body diagram of the exoskeleton

Figure 37 shows the exoskeleton free body diagram, where the upper arm is considered to be fixed at a given angle θ_1. The angle between the upper arm and the forearm is θ_2 with a motion range between 0 and $\frac{\pi}{2}$ rad, the torque applied by the motor is τ, the Load has a range between 0 and 100N, always perpendicular to exoskeleton forearm segment, the sum of the human forearm and exoskeleton forearm masses M is equal to 2.14 kg, the distance between the elbow center and the forearm center of mass L_1 is 0.12m, the length of the forearm L_2 is 0.22m, the forearm moment of inertia J_e is equal to $5.6 \cdot 10^{-3} kg \cdot m^2$.

Table 7: Exoskeleton model parameters

Parameter	Value
Load	0 to 100N
L_1	0.12m
L_2	0.22m
J_e	$5.6 \cdot 10^{-3} kg \cdot m^2$
J_m	$6 \cdot 10^{-5} kg \cdot m^2$
B	1.2732
n	10
K_m	0.533

Equation B.3 shows the dynamics of the exoskeleton:

$$\left(\frac{J_e}{n} + J_m\right) \cdot \ddot{\theta}_m + B \cdot \dot{\theta}_m = \tau + \frac{-L_2 \cdot Load - L_1 \cdot M \cdot g \cdot sin\left(\frac{\theta_m}{n} + \theta_1\right)}{n} \tag{B.3}$$

Where θ_m is the angle of the motor shaft, $J_m = 6 \cdot 10^{-5} kg \cdot m^2$ is the motor moment of inertia, B = 1.2732 is the damping coefficient of the motor, n = 10 is the reduction factor and $K_m = 0.533$ is the electrical current gain of the motor.

Equation B.4 gives the relation between motor input current and output torque:

$$\tau = K_m \cdot I \tag{B.4}$$

Using equations B.2, B.3 and B.4 gives the exoskeleton and human dynamics, without considering human actuation:

$$\left(\frac{J_e}{n} + J_m\right) \cdot \ddot{\theta}_m + B \cdot \dot{\theta}_m = K_m \cdot K_v \cdot V + \frac{-L_2 \cdot Load - L_1 \cdot M \cdot g \cdot sin\left(\frac{\theta_m}{n} + \theta_1\right)}{n} \tag{B.5}$$

B.2 Control

B.2.1 General Characteristics

The action control will be the voltage V applied to the driver of the motor. The load applied to the exoskeleton can vary from 0N to 100N. In this way the user will be able to manipulate different objects without changing the control parameters in a short time span. The controller goal is to control the exoskeleton position while maintaining safety and confort. The range of motion of the elbow joint is from 0 to $\frac{\pi}{2}$ rad while the maximum angular velocity must be around $\frac{\pi}{4}$ rad/s. There must be no overshoot on the movement.

B.2.2 Impedance Control

The first law will be based on impedance control. Impedance control imposes a dynamic behavior to the interaction between the target system and the environment, usually a mass-spring-damper system. Impedance control is suited for tasks that require contact forces without an accurate control of the end-effector position (e.g. grabing an object). That is especially important in biomechanical applications since the human arm is capable of doing delicate tasks without a profound knowledge of necessary forces to be applied to the target objects. One drawback is that whenever an external force is applied on the system the final position of the end-effector will not necessarily be the desired one, instead it controls a combination of force and position. The chosen stiffness for the dynamic system will regulate this trade-off between contact force and position accuracy.

B.2.3 Impedance Control Design

The open-loop system dynamics given by equation B.5, can be rewritten as follows:

$$\ddot{\theta}_m = \frac{-B \cdot \dot{\theta}_m + \frac{-L_2 \cdot Load - L_1 \cdot M \cdot g \cdot sin(\frac{\theta_m}{n} + \theta_1)}{n} + K_v \cdot K_m \cdot V}{\frac{J_e}{n} + J_m} \tag{B.6}$$

Equation B.6 can be organized in the form:

$$\ddot{\theta}_m = f + bu \tag{B.7}$$

Where:

$$f = \frac{-B \cdot \dot{\theta}_m + \frac{-L_2 \cdot Load - L_1 \cdot M \cdot g \cdot sin\left(\frac{\theta_m}{n} + \theta_1\right)}{n}}{\frac{J_e}{n} + J_m} \tag{B.8}$$

$$b = \frac{K_v \cdot K_m}{\frac{J_e}{n} + J_m} \tag{B.9}$$

$$u = V \tag{B.10}$$

The desired closed loop dynamics *to implement an impedance control* is:

$$M_d \cdot (\ddot{\theta}_m - \ddot{\theta}_d) + B_d \cdot (\dot{\theta}_m - \dot{\theta}_d) + K_d \cdot (\theta_m - \theta_d) = -F \tag{B.11}$$

Where M_d, B_d, K_d, θ_d are, respectively, the desired inertia, damping, stiffness and position and the force F is:

$$F = \frac{L_2 \cdot Load}{n} \tag{B.12}$$

Equation B.11 characterizes a mass-spring-damper dynamics that will be imposed to the system by the controller.

By substituting equation B.11 in equation B.7 and rearranging its terms:

$$u = \frac{\ddot{\theta}_m - f}{b} \tag{B.13}$$

$$V = b^{-1}\left(-f + \frac{M_d \cdot \ddot{\theta}_d - B_d \cdot (\dot{\theta}_m - \dot{\theta}_d) - K_d \cdot (\theta_m - \theta_d) - F}{M_d}\right) \tag{B.14}$$

Equation B.14 gives the control law for the system, that can be expressed as (using B.6 - B.12)

$$\begin{aligned} V = \frac{1}{K_v \cdot K_m}(B \cdot \dot{\theta}_m + \frac{L_2 \cdot Load}{n} + \frac{L_1 \cdot M \cdot g \cdot sin(\frac{\theta_m}{n} + \theta_1)}{n} + \\ (\frac{J_e}{n} + J_m)(M_d \cdot \ddot{\theta}_d - B_d(\dot{\theta}_m - \dot{\theta}_d) - K_d(\theta_m - \theta_d) - \frac{L_2 \cdot Load}{n}) \cdot \frac{1}{M_d}) \end{aligned} \tag{B.15}$$

This control law, as it is presented, cancels the nonlinearities of the system by imposing a force that counteracts the gravitational and damping forces and imposes the desired dynamic system behavior to the exoskeleton.

B.2.4 Sliding Mode Control Design

The second applied control law will be the Sliding Mode control. The system dynamics is the same as shown in equation B.3

The desired sliding surface s is:

$$s = \dot{\theta}_m - \dot{\theta}_d + \lambda \cdot (\theta_m - \theta_d) \tag{B.16}$$

The control signal is u and λ is the unique pole of the resulting reduced dynamics of the system when in sliding mode. To achieve the desired controlled dynamics of the system, the u value is as follows (SLOTINE; LI, 1991):

$$u = \hat{b}^{-1}\left(-\hat{f} + \ddot{\theta}_d - \lambda \cdot (\theta_m - \theta_d) - K \cdot sat\left(\frac{s}{\phi}\right)\right) \tag{B.17}$$

Where:

$$\hat{b} = \frac{K_v \cdot K_m}{\frac{J_e}{n} + \hat{J}_m} \tag{B.18}$$

$$\hat{f} = \frac{-B \cdot \dot{\theta}_m + \frac{-L_2 \cdot \hat{Load} - L_1 \cdot M \cdot g \cdot sin(\frac{\theta_m}{n} + \theta_1)}{n}}{\frac{J_e}{n} + \hat{J}_m} \tag{B.19}$$

$\hat{J_m}$ is the motor inertia with measuring error and $\hat{Load}$ is the external load applied to the exoskeleton with measuring error.

In this way, the system acquires the following dynamics in closed loop:

$$\frac{ds}{dt} = (\ddot{\theta}_m - \ddot{\theta}_d) + \lambda \cdot (\dot{\theta}_m - \dot{\theta}_d) \tag{B.20}$$

That is,

$$\begin{aligned} \frac{ds}{dt} = f + b \cdot \hat{b}^{-1} \cdot (-\hat{f}) + b \cdot \hat{b}^{-1} \cdot (\ddot{\theta}_d - \lambda \cdot (\theta_m - \theta_d) + \\ - b \cdot \hat{b}^{-1} \cdot K \cdot sat(\frac{s}{\phi}) - \ddot{\theta_m} + \lambda \cdot (\dot{\theta}_m - \dot{\theta}_d)) \end{aligned} \tag{B.21}$$

In order to guarantee convergence, the control must satisfy the sliding condition:

$$\frac{1}{2}\frac{d(s^2)}{dt} \leq -\eta \cdot |s| \tag{B.22}$$

Equation B.22, using B.21:

$$K \geq \beta \cdot (\eta + F) + (\beta - 1) \cdot |\hat{u}| \tag{B.23}$$

Where,

$$\beta = \sqrt{\frac{b_{max}}{b_{min}}} \tag{B.24}$$

$$F > |f - \hat{f}| \tag{B.25}$$

$$\hat{u} = -\hat{f} + \ddot{\theta}_d - \lambda \cdot (\theta_m - \theta_d) \tag{B.26}$$

B.3 Simulation Results

B.3.1 Impedance Control

By choosing $M_d = 1kg \cdot m^2, B_d = 4N \cdot m \cdot s, K = 4.5N \cdot m$ and $\theta_d = 1rad$ one obtains $\omega_n = \frac{2\pi}{8}$ rad/s the natural frequency of the system, $t_{0-90\%} = 2.4s$ the time the system takes to reach 90% of the final position and the damping factor ζ must be greater than one since there must be no overshoot.

Figures 38 and 39 show the results of a simulation where $\theta_d = 1rad \approx \frac{\pi}{3}$ and external load $= 0$ and 100N, respectively.

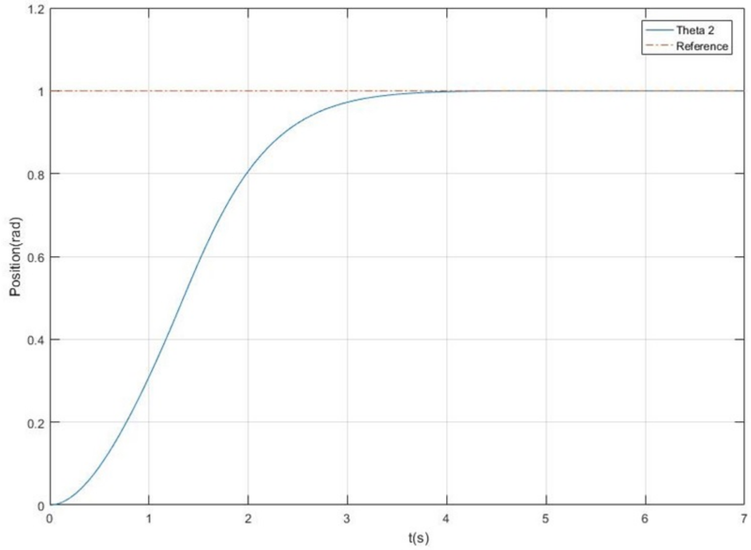

Figure 38: Position θ_2 versus time for an external load $= 0$

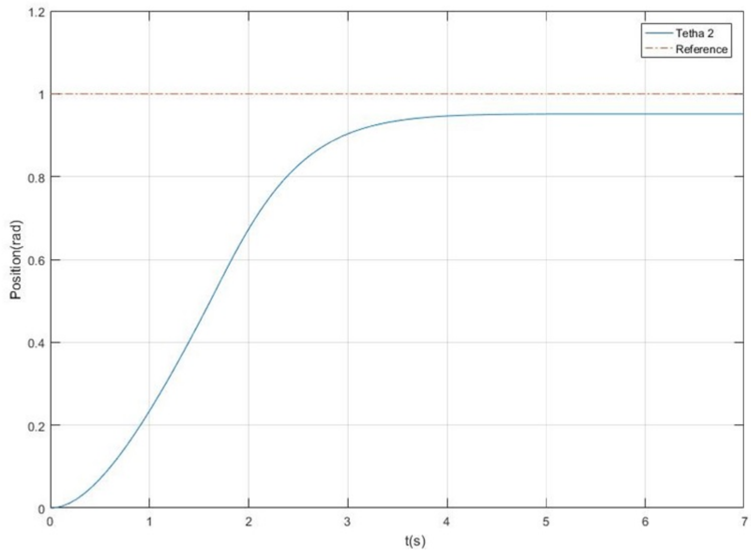

Figure 39: Position θ_2 versus time for an external load $= 100$ N

B.3.2 Sliding Mode Control

Considering the measured load with 30% error and the measured motor inertia with 20% error, that is, $\hat{Load} = 130N$ and $\hat{J}_m = 7.2 \cdot 10^{-5} kg \cdot m^2$, resulting in $\beta = 1.04$, the system was simulated with the following parameters: $\eta = 5rad/s^2, \lambda = 1$ and $\phi = 10rad/s$

and the results for the position and the sliding surface can be found in figures 40 and 41, respectively.

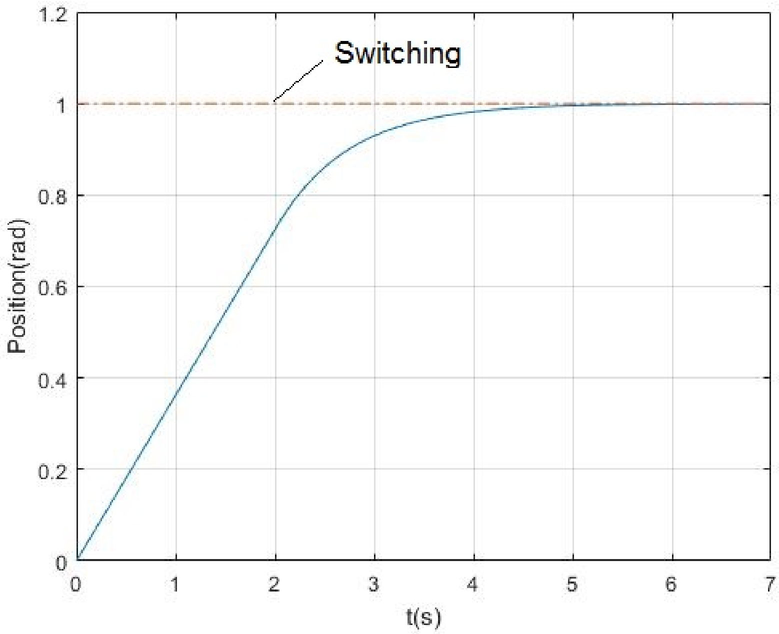

Figure 40: Position θ_2 versus time

B.4 Conclusions

Human limb mechanics are complex and nonlinear. To design a controller that successfully controls the desired movement of the exoskeleton, human and exoskeleton dynamics were modeled. Two different nonlinear control approaches were proposed: Impedance control through feedback linearization and sliding mode control. Both control modes can be adequately applied for exoskeleton control.

Both control approaches have advantages and drawbacks.

The impedance control cannot reach a desired position with utmost accuracy since the external load, by definition, will take the system out of its desired final position and the system parameters must be precisely measured in order to guarantee accurate desired dynamics. Nevertheless, the position error is inferior to 10% of the final position, being sufficient for the application proposed in this work. One advantage of this control is that precise activities can be achieved without a deep knowledge of the environment, the system acquires familiar characteristics in the form of a mass-spring-damper system and it is safer for the user since the controller changes the position of the system when an excessive external load is detected.

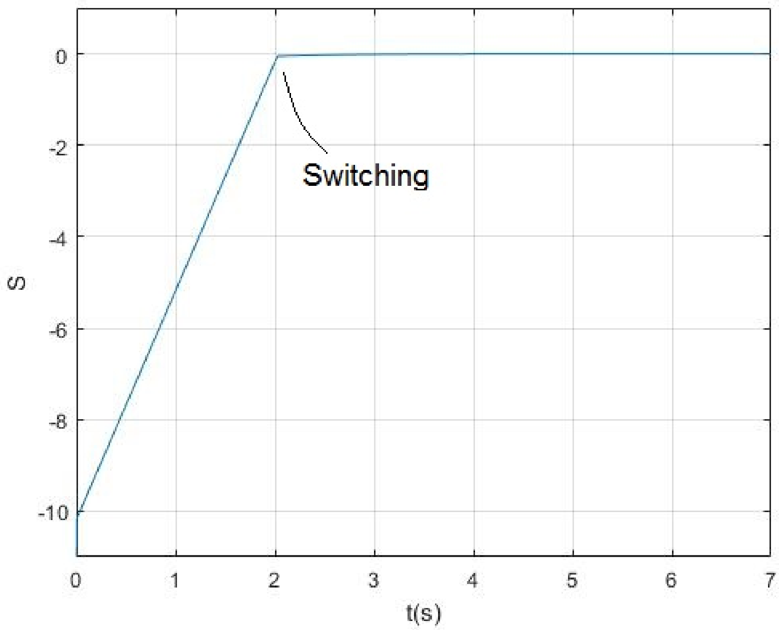

Figure 41: Sliding surface versus time

The sliding mode control can achieve great precision and accuracy of desired position and trajectory and does not require a precise measurement of the system characteristics.

Depending on the application, each one of these control methods could be more appropriate. In the case of a wearable exoskeleton, the impedance control is the most suitable control method, since it offers a dynamic behavior similar to that of a human limb and it is safer for the user. To control an external robotic arm, the sliding mode control can be used since it will cause no harm to the user and it is capable of performing actions with higher accuracy.

Since this work aims to design a controller for an exoskeleton in direct contact with its user, it can be concluded that the impedance control is more appropriate. Even so, the sliding mode control is a good candidate and has been deemed fit for exoskeleton control in past studies (MIRANDA; FORNER-CORDERO, 2013).

ANNEX A – SPARKFUN MUSCLE SENSOR V3 SCHEMATIC

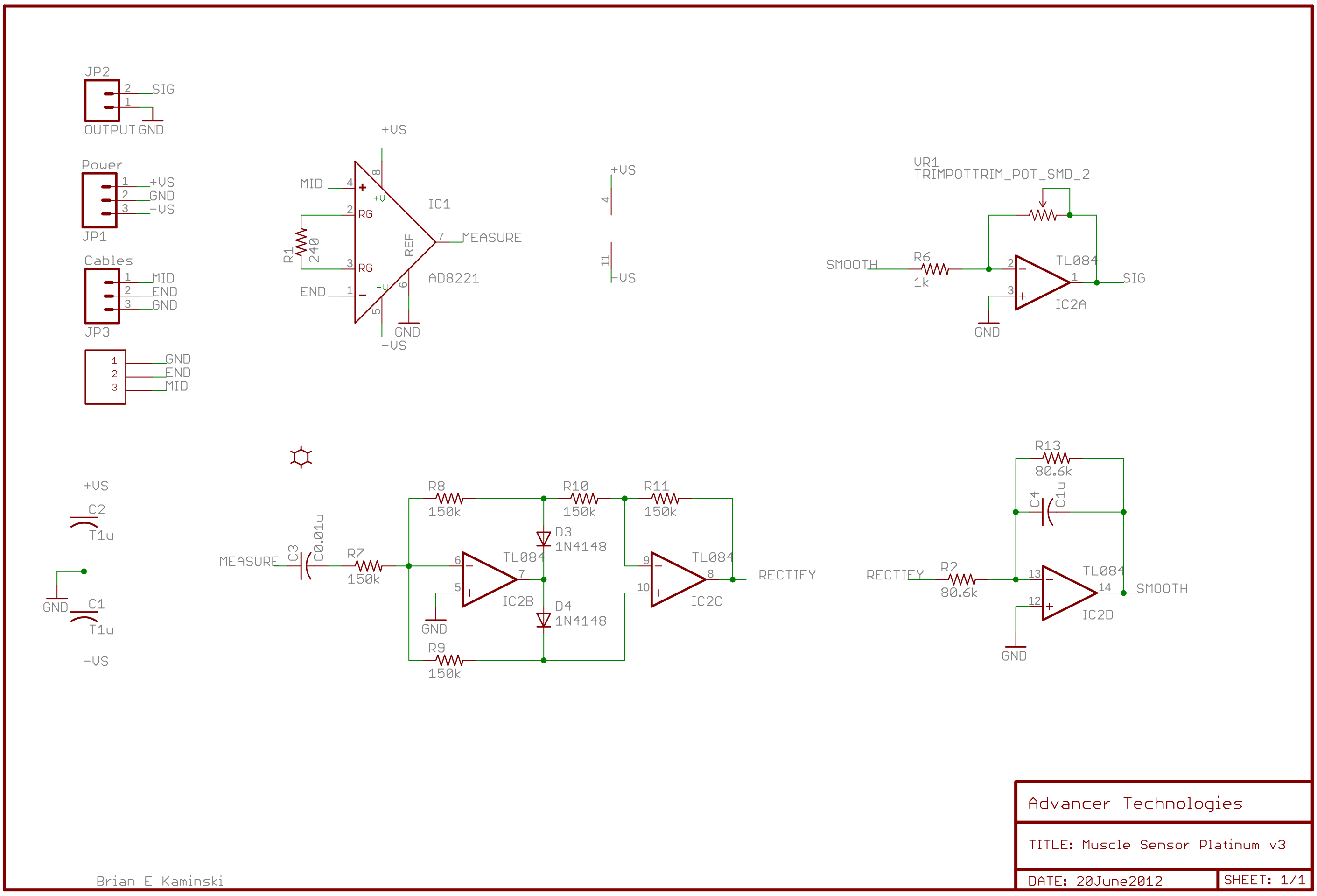

2/4/2013 1:03:11 PM H:\EMG\Muscle Sensor Platinum\v3\Muscle Sensor Platinum v3.3.sch (Sheet: 1/1)

ANNEX B – MODEXO CONTROL HARDWARE SCHEMATICS

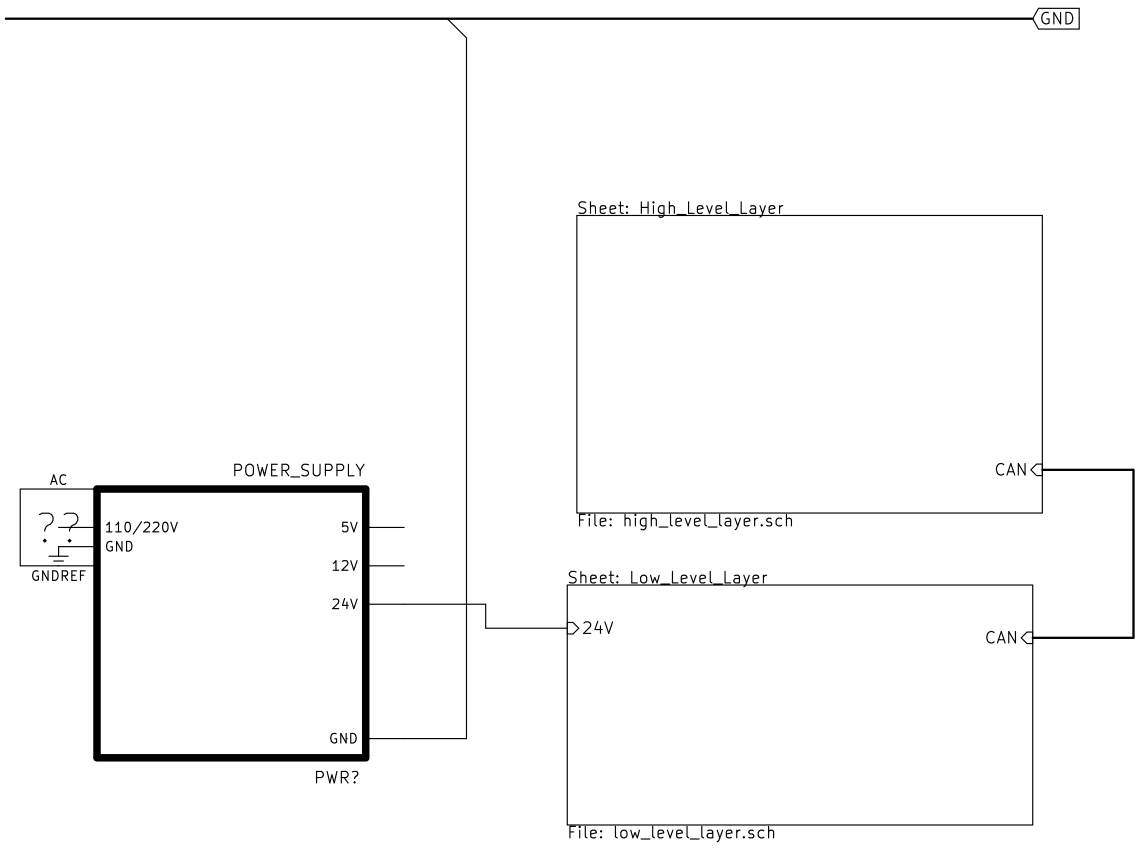

Sheet: /		
File: modexo.sch		
Title:		
Size: A4	Date:	**Rev:**
KiCad E.D.A. eeschema 4.0.4-stable		Id: 1/3

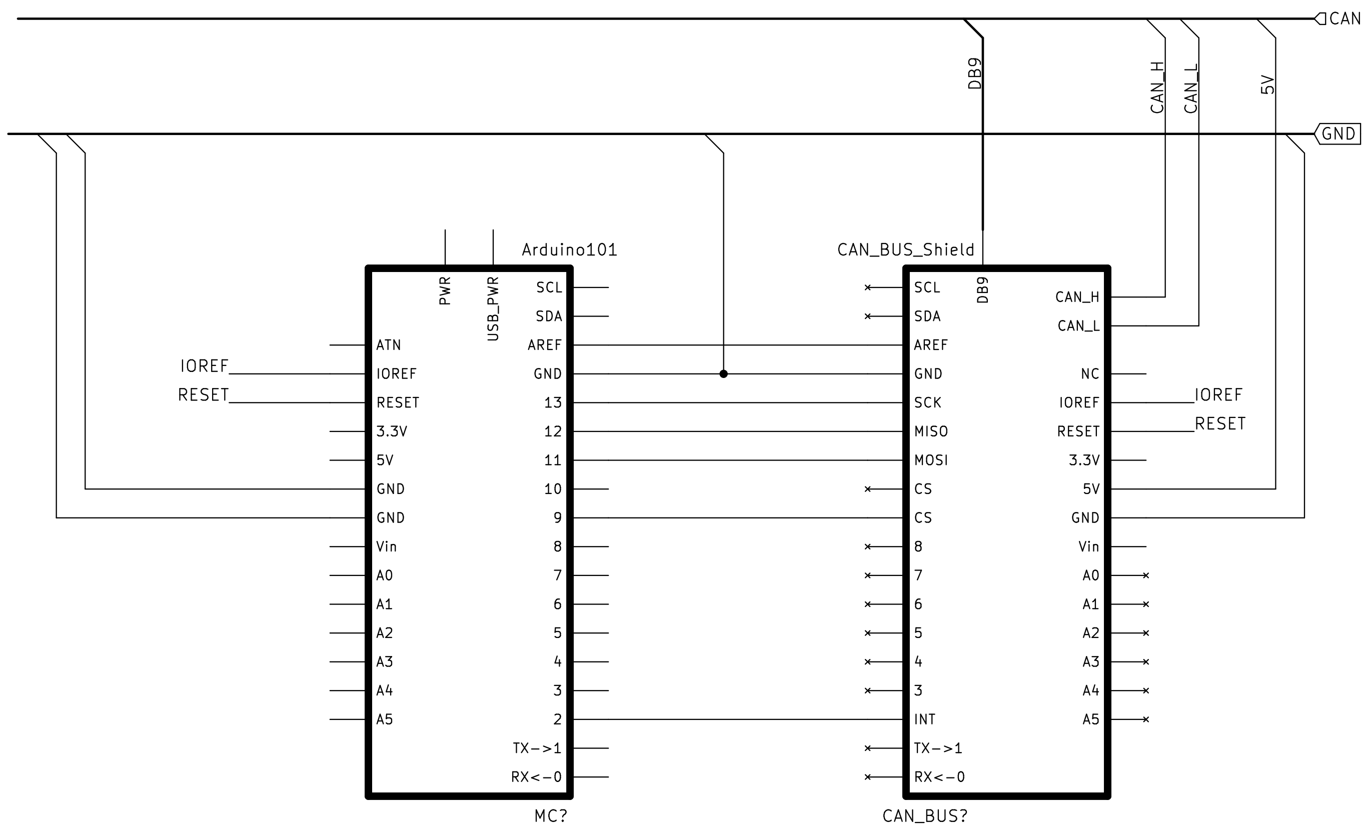

Sheet: /High_Level_Layer/
File: high_level_layer.sch

Title: High Level Layer Communication

Size: A4	Date:	**Rev:**
KiCad E.D.A. eeschema 4.0.4-stable		Id: 2/3

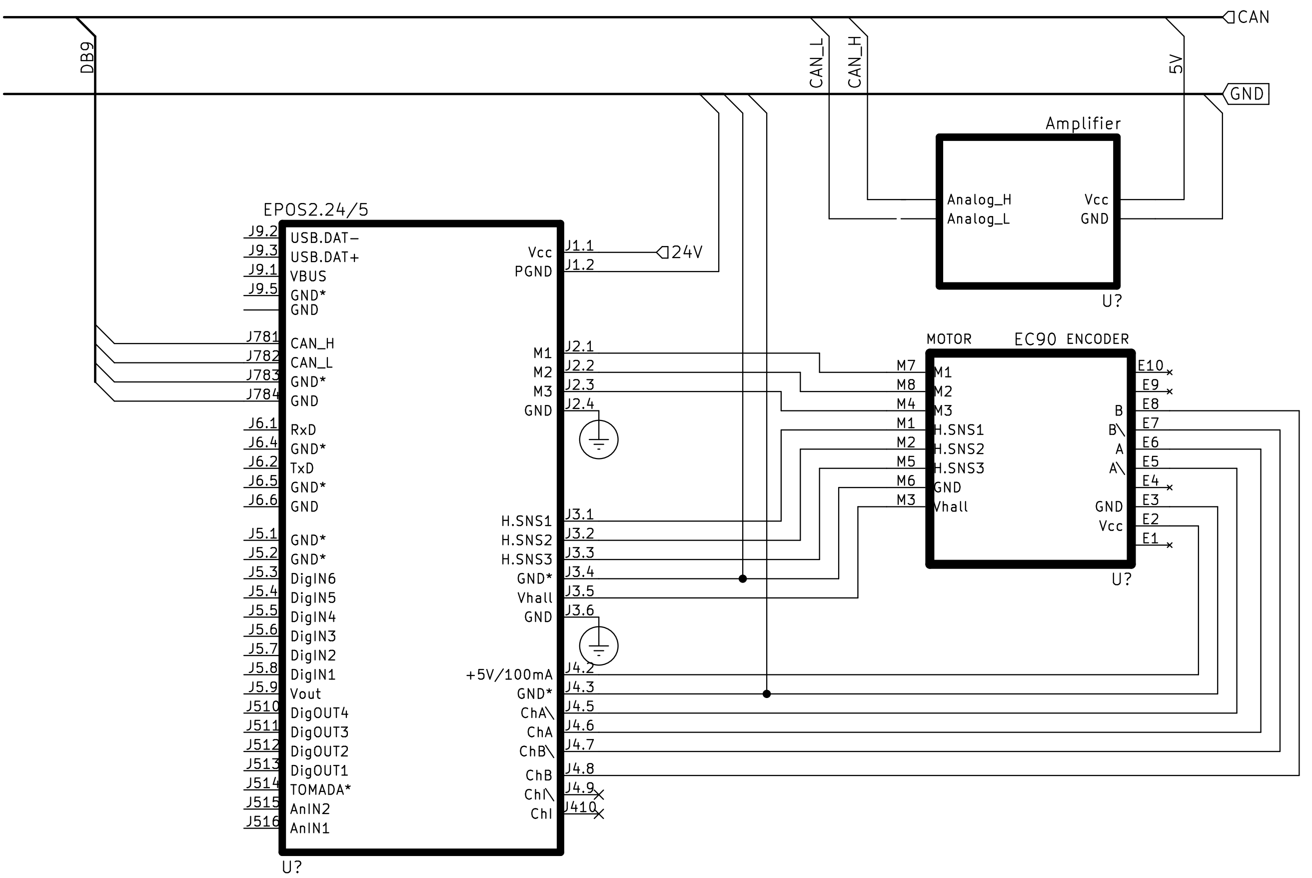

Sheet: /Low_Level_Layer/
File: low_level_layer.sch

Title: Low Level Layer Communication

Size: A4	Date:	**Rev:**
KiCad E.D.A. eeschema 4.0.4-stable		Id: 3/3